



**HAL**  
open science

# Computational and robotic modeling reveal parsimonious combinations of interactions between individuals in schooling fish

Liu Lei, Ramón Escobedo, Clément Sire, Guy Theraulaz

## ► To cite this version:

Liu Lei, Ramón Escobedo, Clément Sire, Guy Theraulaz. Computational and robotic modeling reveal parsimonious combinations of interactions between individuals in schooling fish. *PLoS Computational Biology*, 2020, 16 (3), pp.e1007194. <10.1371/journal.pcbi.1007194>. <hal-03363016v2>

**HAL Id: hal-03363016**

**<https://hal.science/hal-03363016v2>**

Submitted on 2 Oct 2021

**HAL** is a multi-disciplinary open access archive for the deposit and dissemination of scientific research documents, whether they are published or not. The documents may come from teaching and research institutions in France or abroad, or from public or private research centers.

L'archive ouverte pluridisciplinaire **HAL**, est destinée au dépôt et à la diffusion de documents scientifiques de niveau recherche, publiés ou non, émanant des établissements d'enseignement et de recherche français ou étrangers, des laboratoires publics ou privés.



HAL Authorization

# Computational and robotic modeling reveal parsimonious combinations of interactions between individuals in schooling fish

Liu Lei<sup>1,2</sup>, Ramón Escobedo<sup>2</sup>, Clément Sire<sup>3</sup>, Guy Theraulaz<sup>2,\*</sup>

**1** University of Shanghai for Science and Technology, Shanghai, China

**2** Centre de Recherches sur la Cognition Animale, Centre de Biologie Intégrative, Centre National de la Recherche Scientifique (CNRS), Université de Toulouse – Paul Sabatier (UPS), Toulouse, France

**3** Laboratoire de Physique Théorique, CNRS and Université de Toulouse – Paul Sabatier, Toulouse, France

\* guy.theraulaz@univ-tlse3.fr

## Abstract

Coordinated motion and collective decision-making in fish schools result from complex interactions by which individuals integrate information about the behavior of their neighbors. However, little is known about how individuals integrate this information to take decisions and control their motion. Here, we combine experiments with computational and robotic approaches to investigate the impact of different strategies for a fish to interact with its neighbors on collective swimming in groups of rummy-nose tetra (*Hemigrammus rhodostomus*). By means of a data-based agent model describing the interactions between pairs of *H. rhodostomus* (Calovi *et al.*, 2018), we show that the simple addition of the pairwise interactions with two neighbors quantitatively reproduces the collective behavior observed in groups of five fish. Increasing the number of interacting neighbors does not significantly improve the simulation results. Remarkably, and even without confinement, we find that groups remain cohesive and polarized when each agent interacts with only one of its neighbors: the one that has the strongest contribution to the heading variation of the focal agent, dubbed as the “most influential neighbor”. However, group cohesion is lost when each agent only interacts with its nearest neighbor. We then investigate by means of a robotic platform the collective motion in groups of five robots. Our platform combines the implementation of the fish behavioral model and a control system to deal with real-world physical constraints. A better agreement with experimental results for fish is obtained for groups of robots only interacting with their most influential neighbor, than for robots interacting with one or even two nearest neighbors. Finally, we discuss the biological and cognitive relevance of the notion of “most influential neighbors”. Overall, our results suggest that fish have to acquire only a minimal amount of information about their environment to coordinate their movements when swimming in groups.

**Keywords:** collective behavior; flocking; fish school; interaction networks; computational modeling; collective robotics.

## 28 Author Summary

29 How do fish integrate and combine information from multiple neighbors when swimming  
30 in a school? What is the minimum amount of information about their environment  
31 needed to coordinate their motion? To answer these questions, we combine experiments  
32 with computational and robotic modeling to test several hypotheses about how individual  
33 fish could integrate and combine the information on the behavior of their neighbors  
34 when swimming in groups. Our research shows that, for both simulated agents and  
35 robots, using the information of two neighbors is sufficient to qualitatively reproduce the  
36 collective motion patterns observed in groups of fish. Remarkably, our results also show  
37 that it is possible to obtain group cohesion and coherent collective motion over long  
38 periods of time even when individuals only interact with their most influential neighbor,  
39 that is, the one that exerts the most important effect on their heading variation.

## 40 Introduction

41 One of the most remarkable characteristics of group-living animals is their ability to  
42 display a wide range of complex collective behaviors and to collectively solve problems  
43 through the coordination of actions performed by the group members [1–3]. It is now well  
44 established that these collective behaviors are self-organized and mainly result from local  
45 interactions between individuals [4, 5]. Thus, to understand the mechanisms that govern  
46 collective animal behaviors, we need to decipher the interactions between individuals, to  
47 identify the information exchanged during these interactions and, finally, to characterize  
48 and quantify the effects of these interactions on the behavior of individuals [6, 7]. There  
49 exists today a growing body of work that brought detailed information about the direct  
50 and indirect interactions involved in the collective behaviors of many animal groups,  
51 especially in social insects such as ants [8–11] and bees [12, 13].

52 Recently, we introduced a new method to disentangle and reconstruct the pairwise  
53 interactions involved in the coordinated motion of animal groups such as fish schools,  
54 flocks of birds, and human crowds [14, 15]. This method leads to explicit and concise  
55 models which are straightforward to implement numerically. It still remains an open  
56 and challenging problem to understand how individuals traveling in groups combine the  
57 information coming from their neighbors to coordinate their own motion.

58 To answer this question, one first needs to identify which of its neighbors an individual  
59 interacts with in a group, *i.e.*, which are its influential neighbors. For instance, does an  
60 individual always interact with its nearest neighbors, and how many? Most models of  
61 collective motion in animal groups generally consider that each individual is influenced by  
62 all the neighbors located within some spatial domain centered around this individual [16,  
63 17]. This is the case in particular of the Aoki-Couzin model [18, 19] and the Vicsek  
64 model [20]. In the latter, each individual aligns its direction of motion with the average  
65 direction of all individuals that are located within a fixed distance in its neighborhood.  
66 Other models, more directly connected to biological data, consider that the interactions  
67 between individuals are topological and that the movement of each individual in the  
68 group only relies on a finite number of neighbors. This is in particular the case for the  
69 work on starling flocks [21, 22] and on barred flagtails (*Kuhlia mugil*) [23]. In golden  
70 shiners (*Notemigonus crysoleucas*), another work has sought to reconstruct the visual  
71 information available to each individual fish during collective evasion maneuvers [24].  
72 In this species, it has been shown that the transmission of behavior in a school was  
73 best described by a model in which the response probability of a fish depends on the  
74 fraction of active neighbors perceived by that fish. However, because of the cognitive  
75 load that is required for an individual to constantly monitor the movements of a large  
76 number of neighbors, it has been suggested that animals may focus their attention on

77 a small subset of their neighbors [25–27]. In a previous work, we found experimental  
 78 evidence that supports this assumption. In groups of rummy nose tetras (*Hemigrammus*  
 79 *rhodostomus*) performing collective U-turns, we found that, at any time, each fish pays  
 80 attention to only a small subset of its neighbors, typically one or two, whose identity  
 81 regularly changes [28]. However, we still do not know if the same pattern of interaction  
 82 holds true when fish are schooling, *i.e.*, when individuals are moving together in a highly  
 83 polarized manner and not performing some collective maneuver.

84 Once the influential neighbors of a focal fish have been identified, one must then  
 85 understand how this individual combines the information about the behavior of these  
 86 neighbors. The most common assumption is that animals respond by averaging pairwise  
 87 responses to their neighbors (with added noise) [16–18]. However, existing work shows  
 88 that the integration of information might be much more complex. In golden shiners,  
 89 Katz *et al.* [29] have shown that the combined effect of two neighbors on a fish response  
 90 is close to averaging for turning, but somewhere between averaging and adding for speed  
 91 adjustments. This observation brings us back to an often neglected factor which is the  
 92 impact of the physical constraints imposed on a fish movement by their body. Fish  
 93 mainly achieve collision avoidance through the control of their speed and orientation  
 94 at the individual level. However, existing models seldom treat collision avoidance in a  
 95 physical way and most models assume that individuals move at a constant speed [6].  
 96 This is the main reason why these models cannot be directly implemented in real physical  
 97 robotic systems [30].

98 To better understand how individuals integrate and combine interactions with their  
 99 neighbors in a group of moving animals, we first analyze the dynamics of collective  
 100 movements in groups of five *H. rhodostomus* moving freely in a circular tank. Then,  
 101 we investigate different strategies for combining pairwise interactions between fish  
 102 and analyze their impact on collective motion. To do that, we use the data-driven  
 103 computational model developed by Calovi *et al.* [14] that describes the interactions  
 104 involved in the coordination of burst-and-coast swimming in pairs of *H. rhodostomus*,  
 105 and a robotic platform that also allows us to investigate the impact of direction and  
 106 speed regulation, and of collision avoidance. Finally, we compare the predictions of the  
 107 computational and robotics models with the experiments conducted under the same  
 108 conditions with groups of fish.

## 109 Results

110 We collect three sets of data corresponding to *i*) our experiments with  $N = 5$  fish  
 111 (*H. rhodostomus*), *ii*) our numerical simulations of the model derived in [14], and *iii*) our  
 112 experiments using the robotic platform with  $N = 5$  robots (see Fig. 1, S1 Video and  
 113 S2 Video), from which we extract the trajectories of each individual (S3 Video). We  
 114 characterize the collective behavior of fish, agents, and robots by means of five main  
 115 quantities:

- 116 • the group cohesion  $C(t)$  at time  $t$ , which characterizes the effective radius of the  
 117 group, and hence its compactness;
- 118 • the group polarization  $P(t)$ , which quantifies the coordination of the headings of  
 119 the individuals ( $P(t) = 1$ , if all individuals are perfectly aligned;  $P \sim 1/\sqrt{N}$ , if  
 120 the  $N$  individuals have uncorrelated headings,  $P$  becoming small only for large  
 121 group size  $N$ , but being markedly lower than 1 for any  $N \geq 5$ );
- 122 • the distance  $r_w^B(t)$  of the barycenter  $B$  of the group from the wall of the tank,  
 123 which is only small compared to the radius of the tank if individuals move together  
 124 *and* along the wall of the tank;

- 125 • the relative orientation  $\theta_w^B(t)$  of the barycenter of the group with respect to the  
126 wall of the tank, which in particular characterizes whether the group is collectively  
127 swimming parallel to the wall of the tank (then,  $|\theta_w^B| \approx 90^\circ$ );
- 128 • the counter-milling index  $Q(t)$ , which measures the relative direction of rotation of  
129 individuals inside the group (around the barycenter) with respect to the direction  
130 of rotation of the group around the center of the tank (see S4 Video).

131 The Materials and Methods section and Figs. 2 and 3 provide the precise mathematical  
132 definition of these quantities. Moreover, we used the Hellinger distance (see Materials  
133 and Methods) between two probability distribution functions (PDF) in order to quantify  
134 the (dis)similarity between PDF obtained in fish experiments and the corresponding  
135 PDF obtained in the fish model (see Table 1) and in robot experiments (see Table 2)

136 *H. rhodostomus* presents a burst-and-coast swimming mode, where a fish suddenly  
137 accelerates along a new direction (“kick”; see Fig. 1B, and S1 Video and S3 Video)  
138 and then glides passively until the next kick, along an almost straight line, a gliding  
139 phase during which the speed approximately decays exponentially [14]. The fish model  
140 derived in [14] explicitly implements this swimming mode and returns as the main  
141 information the new heading direction of the focal fish after each kick, which is controlled  
142 by its environment (wall of the tank, another fish). The interaction between a fish  
143 and the wall, and the interaction between two fish have been precisely extracted from  
144 actual experiments with *H. rhodostomus* [14]. The original procedure for extracting the  
145 interactions introduced in [14] exploited a large data set of  $\sim 300000$  kicks for one-fish  
146 trajectories (in tanks of 3 different radii) and  $\sim 200000$  kicks for two-fish trajectories,  
147 amounting effectively to a total of 70 hours of exploitable data. The measured interactions  
148 were then directly implemented in the model, which is hence not just a phenomenological  
149 model with mere guessed, albeit reasonable, interactions. Note however that the analysis  
150 in [14] does not provide any insight about how these interactions are combined in groups  
151 of more than two fish.

152 The interaction between two fish was shown to be a combination of a repulsive (at  
153 short distance of order 1 BL – body length) and a long-range (in particular, compared to  
154 zebrafish [15]) attractive interaction at larger distance, and of an alignment interaction  
155 which tends to make the two fish align their heading direction. The attraction and  
156 alignment interaction functions determine the new heading angle of the focal fish in  
157 terms of the instantaneous relative state of the two fish, characterized by the distance  
158 between them, the viewing angle with which the neighbor is perceived by the focal fish,  
159 and their relative orientation (see Fig. 2). The additional change in heading angle due  
160 to the repulsive interaction between a fish and the wall of a circular tank is expressed in  
161 terms of the distance and relative angle of the fish to the wall (see Fig. 2). Finally, in  
162 addition to the fish-wall and fish-fish interactions, the change in heading angle includes  
163 a stochastic contribution describing the spontaneous fluctuations in the motion of the  
164 fish. In [14], the model was shown to quantitatively reproduce many fine measurable  
165 quantities in one-fish and two-fish experiments, ultimately producing a very precise  
166 description of the motion of one or two fish. For the sake of completeness, the model  
167 and its fish-wall and fish-fish interaction functions are summarized in the Materials and  
168 Methods section (Eqs. (4–15); see [14] for a more detailed description and justification  
169 of the model; see [14, 15] for the extraction procedure of the interactions).

170 When more than two fish are swimming in the tank ( $N > 2$ ), the social pairwise  
171 interactions must be combined. In the framework of the fish model, it is natural to assume  
172 that the heading angle change of a focal fish is the sum of the pairwise contributions of  
173 *some* of its  $N - 1$  neighbors. The resulting interaction thus depends on two factors: the  
174 *number*  $k$  of considered neighbors and the *strategy* to select them.

175 We explore three different strategies of interaction between individuals and their  
176 neighbors in groups of size  $N = 5$ , comparing actual fish experiments with the resulting

177 fish model and the robotic platform. In the latter, the robots are programmed with the  
 178 fish model and a control procedure to resolve collisions. The first strategy is based on  
 179 the *distance*, so that individuals interact with their  $k$  nearest neighbors, with  $k = 1, 2, 3$ .  
 180 The second strategy is a *random* strategy, where the  $k$  neighbors are randomly sampled  
 181 among the other  $N - 1$  individuals. Finally, the third strategy is based on the *influence*,  
 182 defined below, where the  $k$  selected neighbors are those having the largest influence on  
 183 the focal individual (as determined by the precise two-fish model of [14]). We also study  
 184 the cases where there is no interaction between individuals ( $k = 0$ ), and where each  
 185 individual interacts with all its neighbors ( $k = 4$ ).

186 The *influence*  $\mathcal{I}_{ij}(t)$  of a neighbor  $j$  on a focal individual  $i$  at time  $t$  is defined as the  
 187 intensity of the contribution of this neighbor  $j$  to the instantaneous heading variation  
 188 of the focal individual  $i$ , as given by the firmly tested two-fish model of [14]. The  
 189 influence  $\mathcal{I}_{ij}(t)$  depends on the relative state of the neighbor  $j$  with respect to the focal  
 190 individual  $i$ , determined by the triplet  $(d_{ij}, \psi_{ij}, \phi_{ij})$ , where  $d_{ij}$  is the distance between  
 191 individuals  $i$  and  $j$ ,  $\psi_{ij}$  is the viewing angle with which  $i$  perceives  $j$  (*i.e.*, the angle  
 192 between the velocity of  $i$  and the vector  $\vec{i}j$ ), and  $\phi_{ij}$  is the difference of their heading  
 193 angles, a measure of the alignment between  $i$  and  $j$  (see Fig. 2). The influence  $\mathcal{I}_{ij}(t)$  is  
 194 evaluated at each kicking time of individual  $i$  by means of the analytical expressions of  
 195 the pairwise interaction functions derived in [14] for fish swimming in pairs, according  
 196 to Eq. (9) in the Materials and Methods section.

197 To prevent cognitive overload, a reasonable assumption is that individual fish filter  
 198 the information from their environment and thus limit their attention to a small set of  
 199 their most salient neighbors [25–27] (to be followed; or to be avoided, by moving away  
 200 or by aligning their headings), making the notion of most influential neighbors quite  
 201 natural.

202 The model for  $N > 2$  agents thus proceeds as follows: at the time when the agent  
 203 performs a new kick, its change in heading angle is calculated by adding the effects of  
 204 the wall and the spontaneous noise to the effects of the  $k$  neighbors selected among the  
 205 other  $N - 1$  individuals according to one of the three strategies presented above:

- 206 • by calculating the instantaneous distance between the focal individual  $i$  and each  
 207 of its  $N - 1$  neighbors and selecting the  $k$  nearest neighbors (strategy 1; NEAREST);
- 208 • by randomly sampling  $k$  individuals among the  $N - 1$  neighbors of  $i$  (strategy 2;  
 209 RANDOM);
- 210 • by calculating the instantaneous influence  $\mathcal{I}_{ij}(t)$  for each neighbor  $j$  of  $i$  and  
 211 selecting the  $k$  neighbors with the largest influence (strategy 3; MOST INFLUENTIAL).

212 The strategy is thus characterized by the number  $k$  of neighbors taken into account in  
 213 the social interaction and the criterion used to select them (NEAREST, RANDOM, or MOST  
 214 INFLUENTIAL). The strategy remains unchanged along the whole simulation. However,  
 215 the identity of the neighbors selected to interact with a given agent can change from one  
 216 kick to another, and must be updated at each kicking time of this agent. For instance,  
 217 when using the NEAREST strategy with  $k = 2$  in a group of  $N = 5$  agents, the agents  
 218 taken into account in the social interaction in the  $n$ -th kick of agent 1 can be the agents 2  
 219 and 3, and the agents 4 and 3 in its  $(n + 1)$ -th kick. In order to select these  $k$  neighbors at  
 220 a specific kick, the  $N - 1$  agents must be sorted according to the criterion corresponding  
 221 to the strategy used in the simulation. This sorting process is carried out at each kicking  
 222 time of the focal agent, independently of the state (kicking or gliding) of the other agents.  
 223 If  $N$  is so large that the computational cost of this process becomes prohibitive, a more  
 224 efficient algorithm can be implemented, such as keeping track of the agents that were  
 225 selected in the most recent kicks and exploiting grid algorithms to identify neighbors.

226 These interaction strategies explore different ways for an individual to focus its  
 227 attention on the most relevant stimuli (*i.e.*, neighbors).

228 **Collective behavior in fish experiments**

229 Fish form cohesive groups with an average cohesion  $C \approx 5$  cm (Fig. 4). They are highly  
 230 polarized, with the 5 fish swimming almost in the same direction (large peak at  $P \approx 1$   
 231 in the distribution of  $P$ ; Fig. 5). In some instances, groups are observed in which  
 232 one fish swims in the opposite direction to that of the other four, as shown by the  
 233 small bump at  $P \approx 0.6$  in Fig. 5. Indeed, in this situation, the polarization is close  
 234 to  $P \approx |1 + 1 + 1 + 1 - 1|/5 = 0.6$ . Even less frequent are situations where two fish  
 235 swim in the opposite direction to that of the other three, as shown by the very small  
 236 bump near  $P \approx |1 + 1 + 1 - 1 - 1|/5 = 0.2$ . The density maps of polarization  $P$  with  
 237 respect to cohesion  $C$  (panels labeled “FISH” in S1 Fig–S4 Fig) allow to visualize the  
 238 correlations between both quantities, and will permit a comparison with the predictions  
 239 of the fish model and the results of the robot experiments for the three interaction  
 240 strategies considered here.

241 Groups of 5 fish rotate clockwise (CW) or counter-clockwise (CCW) along the tank  
 242 wall for long periods and remain close to the border of the tank, the group barycenter  
 243 being at a typical distance  $r_w^B \approx 7$  cm from the wall (Fig. 6). Therefore, the group swims  
 244 almost always parallel to the nearest wall, with a relative angle to the wall of the heading  
 245 of the barycenter close to  $|\theta_w^B| \approx 90^\circ$  (Fig. 7). In fact, the peak in the PDF of  $|\theta_w^B|$  is  
 246 slightly below  $90^\circ$ , since the fish are more often going toward the wall than away from  
 247 it [14].

248 We also find a collective pattern where individual fish rotate around the barycenter  $B$   
 249 of the group in a direction which is *opposite* to the direction of rotation of the group around  
 250 the center  $T$  of the tank (see Fig. 3 and S4 Video). We call this collective movement a  
 251 *counter-milling behavior*, and define the instantaneous degree of counter-milling  $Q(t)$  as  
 252 a measure in  $[-1, 1]$  of the intensity with which both rotation movements are in opposed  
 253 directions (see the Materials and Methods section for the precise mathematical definition  
 254 of  $Q(t)$  and its general interpretation). When  $Q(t) < 0$ , the fish rotate around their  
 255 barycenter  $B$  in the opposite direction to that of the group around  $T$  (*counter-milling*),  
 256 while when  $Q(t) > 0$ , the fish rotate in the same direction around  $B$  as the group rotates  
 257 around  $T$  (*super-milling*). Fig. 8 shows that the fish exhibit a counter-milling behavior  
 258 much more frequently than a super-milling behavior. Counter-milling behaviors result  
 259 from the fact that fish located at the front of the group have to reduce their speed as  
 260 they get closer to the wall of the tank. Fish located at the back of the group (that  
 261 are generally farther from the wall [14]) move faster and outrun the slowing down fish,  
 262 ultimately relegating them to the back of the group. This process gives rise to the  
 263 rotation of individual fish around the group center, in the opposite direction to the one  
 264 that the group displays around the tank (Fig. 3). This collective behavior resembles a  
 265 coordinated swimming by relays which is nevertheless due to simple physical constraints,  
 266 as already reported on wolf-packs hunting preys moving in circles [31].

267 **Simulation results of the computational model**

268 **Collective motion in a circular tank**

269 Panels (ABC) of Figs. 4–8 show the probability distribution functions for our 5 quantifiers  
 270 as obtained in numerical simulations of the fish model. The panels correspond respectively  
 271 to the strategy in which agents interact with their  $k$  nearest neighbors (A), with  
 272  $k$  neighbors chosen randomly (B), and with  $k$  neighbors selected according to their  
 273 influence on the focal agent (C). For these three strategies (NEAREST; RANDOM; MOST  
 274 INFLUENTIAL), we have considered all the possible values of the number of interacting  
 275 neighbors,  $k = 1, 2, 3$ , together with the case where there is no interaction between  
 276 agents ( $k = 0$ ) and the case where each agent interacts with every other agent ( $k = 4$ ).

277 For comparison purposes, we have rescaled the distance corresponding to the model  
 278 by a factor  $\lambda_M = 0.87$ . This value is the minimizer of the  $l_1$ -norm of the difference  
 279 between the PDF of group cohesion for fish data, and the PDF of group cohesion for the  
 280 simulation data produced by the model when using the strategy involving the  $k = 2$  most  
 281 influential neighbors. Noticeably, the fact that the value of  $\lambda_M$  is close to 1 indicates  
 282 that the model produces a quite satisfactory quantitative approximation to the data of  
 283 real fish. This rescaling procedure only affects the PDF of  $C$  and  $r_w^B$ , and not the PDF  
 284 of  $P$ ,  $\theta_w^B$ , and  $Q$  (3 quantities invariant by a change of distance scale).

285 When  $k = 0$ , there is no interaction between agents and, as expected, one does not  
 286 observe any compact group: individuals turn independently around the tank remaining  
 287 close and parallel to the wall (as expected for fish swimming alone [14]). Their position  
 288 and rotation direction along the walls are uncorrelated, and the individuals are scattered  
 289 along the border (cohesion peaked around  $C \approx 18$  cm;  $r_w^B \approx 15$  cm), with an almost flat  
 290 PDF for  $\theta_w^B$  (random orientation of the barycenter with respect to the wall). This results  
 291 in a bell-shaped probability distribution function PDF for the polarization  $P$ , vanishing  
 292 at  $P = 1$  (Figs. 4–7).

293 For  $k = 1$ , whatever the strategy used to select the interacting neighbor (the nearest  
 294 one; a randomly selected one; the most influential one), the dynamics immediately  
 295 reveals that interactions are at play, with groups becoming more cohesive (Fig. 4) and  
 296 more polarized (Fig. 5) than for  $k = 0$ . Yet, the NEAREST strategy still leads to a very  
 297 broad PDF of the group cohesion  $C$ , with a substantial weight near the maximal value  
 298 of  $C \sim 20$  cm obtained for  $k = 0$ , indicating that the group often breaks into parts. For  
 299 the RANDOM and MOST INFLUENTIAL strategies, the weight at large distance in the PDF  
 300 of  $C$  is absent, but the PDF are still broader than in fish experiments. As confirmed by  
 301 the Hellinger distance quantifier (see Table 1 and Materials and Methods), the MOST  
 302 INFLUENTIAL strategy clearly leads to the sharper distribution of  $C$  (peaked around  
 303  $C \approx 6.5$  cm, compared to  $C \approx 10$  cm for the RANDOM strategy). The next section will  
 304 show that, contrary to the NEAREST strategy, the MOST INFLUENTIAL strategy with  
 305  $k = 1$  can lead to compactness of the group even for larger groups ( $N = 6-70$ ) moving  
 306 in an *unbounded* domain. As for the group polarization  $P$  (Fig. 5), the three strategies  
 307 lead to a PDF clearly peaked near  $P \approx 0.9$  (and a smaller peak near  $P \approx 0.6$ ; see above),  
 308 yet certainly not as peaked near  $P = 1$  as the PDF for fish experiments. Again, the  
 309 MOST INFLUENTIAL strategy leads to the best agreement with fish experiments (see  
 310 Table 1), although the difference between strategies is not as marked as for the group  
 311 cohesion. For the three strategies, the barycenter of the group is closer to the border  
 312 and moves more parallel to the wall (Figs. 6 and 7). Counter-milling is obtained for  
 313 the three strategies with comparable PDF (Fig. 8; see also S5 Fig), quite similar to the  
 314 one obtained in fish experiments (we will see that the agreement unfortunately worsens  
 315 when increasing  $k$ ; see Table 1). Polarization vs cohesion density maps confirm that the  
 316 NEAREST and RANDOM strategies are insufficient to convey the necessary information to  
 317 reach the degree of cohesion and polarization (and their correlation) observed in groups  
 318 of fish (S1 Fig, S2 Fig). The MOST INFLUENTIAL strategy density maps for  $k = 1$  already  
 319 present the main features of the fish experiments, despite a still too broad spreading  
 320 in the  $(C, P)$  plane. Overall, for  $k = 1$ , the MOST INFLUENTIAL strategy gives rise to  
 321 significantly better results than the NEAREST and RANDOM strategies (see Table 1).

322 For  $k = 2$ , the three strategies lead to a collective behavior in much better agreement  
 323 with the fish experiments (see Table 1). In particular, the NEAREST strategy now system-  
 324 atically leads to compact groups, with a PDF of the group cohesion  $C$  (Fig. 4) similar  
 325 to the one obtained for the RANDOM strategy (both peaked around  $C \approx 6.5$  cm). The  
 326 MOST INFLUENTIAL strategy produces a PDF in good agreement with fish experiments  
 327 (both sharply peaked around  $C \approx 5$  cm). The PDF of the polarization is now sharply  
 328 peaked at  $P = 1$  for the three strategies, with a slightly lower level of polarization for

329 the RANDOM strategy compared to the two others (see Fig. 5 and Table 1). Like in the  
 330 case  $k = 1$ , the distance and alignment of the group with respect to the wall are better  
 331 recovered for the NEAREST strategy (Figs. 6 and 7; Table 1), the two other strategies  
 332 leading to slightly broader PDF but much narrower compared to the case  $k = 1$ . The  
 333 counter-milling  $Q$  is enhanced for the three strategies compared to the case  $k = 1$  and  
 334 appears stronger than for fish experiments (Fig. 8). The deterioration of the model  
 335 results for the counter-milling compared to  $k = 1$  and experiments suggests that the  
 336 internal structure of a fish group is more rigid than predicted by the model, actual fish  
 337 behaving closer to particles rotating on a vinyl record (see the interpretation of  $Q$  in  
 338 Materials and Methods). Compared to the case  $k = 1$ , where they were particularly far  
 339 from the experimental maps, polarization vs cohesion density maps for the NEAREST  
 340 and RANDOM strategies and  $k = 2$  show a correlation between  $P$  and  $C$  in much better  
 341 agreement with experiments (S1 Fig, S2 Fig). The MOST INFLUENTIAL strategy results,  
 342 already fair for  $k = 1$ , also improve. The NEAREST strategy leads to the best agreement  
 343 with experiments in the representation of S1 Fig, while the MOST INFLUENTIAL strategy  
 344 leads to the best results in the representation of S2 Fig.

345 When interacting with  $k = 3$  neighbors, the results are almost identical for the  
 346 three strategies because neighbors are the same a high percentage of the time. For two  
 347 (respectively, three) given strategies, the selected neighbors are exactly the same 25% of  
 348 the time (respectively, 6.25%); they have at least 2 neighbors in common 75% of the  
 349 time (respectively, 93.75%); there is always at least one neighbor in common. Interacting  
 350 with the 3 nearest neighbors instead of 2 only improves the group cohesion (see Table 1  
 351 and Fig. 4), while using the 3 most influential ones, instead of 2, does not improve  
 352 significantly any of the measures, including density maps (S1 Fig, S2 Fig). As already  
 353 noted for  $k = 2$ , the counter-milling remains too pronounced compared to experiments  
 354 for the three strategies and  $k = 3$  (see Fig. 8 and S5 Fig).

355 Finally, interacting with  $k = 4$  neighbors does not significantly change the results  
 356 obtained for  $k = 3$  (see Figs. 4–8 and Table 1).

### 357 Collective motion of 5 agents in an unbounded domain

358 The model allows us to simulate the condition where agents are swimming in an un-  
 359 bounded domain by removing the interaction with the wall. This condition is particularly  
 360 interesting to assess the impact of the confinement of the agents due to the arena on  
 361 group cohesion and polarization.

362 Figs. 9 and 10 show respectively the time evolution of group cohesion and polarization  
 363 for the MOST INFLUENTIAL strategy (Panels AD) and the NEAREST strategy (Panels BE),  
 364 and for  $k = 1$  to 4. Despite the absence of confinement due to the wall, all the strategies  
 365 except the one that consists in interacting only with the nearest neighbor ( $k = 1$ ) allow  
 366 the group to remain cohesive and polarized for more than 2.5 hours ( $\approx 10^4$  kicks) in  
 367 numerical simulations (see Figs. 9ABC and 10AB). When agents only interact with their  
 368 most influential neighbor, the group is highly cohesive ( $C \approx 0.1$  m, Fig. 9A), but less  
 369 than in the arena ( $C \approx 0.07$  m, Fig. 4C). However, the polarization is higher when the  
 370 group swim in an unbounded domain (mean of  $P \approx 0.93$ , Fig. 10A) in comparison to  
 371 the arena (mean of  $P \approx 0.78$ , Fig. 5C). Therefore, the confinement due to the arena  
 372 reinforces the group cohesion and weakens the group polarization, which still remains at  
 373 a high level for the MOST INFLUENTIAL strategy.

374 However, when agents only interact with their first nearest neighbor, the group  
 375 disintegrates very quickly and then diffuses, with  $C^2(t)$  growing linearly with the time  $t$   
 376 (Fig. 9C), and  $P(t)$  oscillating around 0.6 (Fig. 10B). Compact groups are recovered for  
 377 the NEAREST strategy with  $k = 2, 3$ , but the MOST INFLUENTIAL strategy systematically  
 378 leads to more cohesive and more polarized groups (Fig. 9AB).

379 In order to better understand to what extent the group cohesion depends on the

380 interaction strategy and/or on the long-range nature of the attraction [14], we have  
 381 also simulated the model by truncating the attraction interaction between two agents  $i$   
 382 and  $j$  when their distance  $d_{ij}$  is greater than a cut-off distance  $d_{\text{cut}}$ :  $F_{\text{Att}}(d_{ij}) = 0$ , if  
 383  $d_{ij} > d_{\text{cut}}$ , where  $F_{\text{Att}}$  is defined in Eq. (10) of the Materials and Methods section. When  
 384  $d_{\text{cut}}$  decreases below some critical value  $d_{\text{cut}}^*$ , we expect that the group will break and  
 385 that the agents will ultimately freely diffuse, illustrating the importance of the range  
 386 of the attraction interaction to ensure the cohesion of the group (see Fig. 9DE) and  
 387 Fig. 10DE).

388 For the MOST INFLUENTIAL strategy with  $k = 1$ , the group remains highly cohesive  
 389 (Fig. 9D) and highly polarized (Fig. 10D) for  $d_{\text{cut}} > d_{\text{cut}}^* \approx 0.9$  m. For  $k = 2, 3$ ,  
 390 and 4,  $d_{\text{cut}}^*$  is found to be slightly smaller than for  $k = 1$  ( $d_{\text{cut}}^* \approx 0.8$  m; Fig. 9D). For  
 391 the NEAREST strategy with  $k = 2$  (the group is never cohesive for  $k = 1$ , even for  
 392  $d_{\text{cut}} = \infty$ ; see above), we find  $d_{\text{cut}}^* \approx 3.5$  m (Fig. 9E), much higher than for  $k = 1$  in the  
 393 MOST INFLUENTIAL strategy. Here, we clearly see that even at a smaller  $k$ , the MOST  
 394 INFLUENTIAL strategy is much more effective than the NEAREST strategy in ensuring  
 395 the cohesion of the group, for finite-range attraction cut-off at  $d_{\text{cut}}$ . For  $k = 3$ , the  
 396 NEAREST strategy leads to a critical cut-off  $d_{\text{cut}}^* \approx 0.9$ , of the same order as for the MOST  
 397 INFLUENTIAL strategy (for  $k = 3$ , the involved neighbors are often the same for both  
 398 strategies; see above).

399 In conclusion, for groups of 5 agents in an unbounded domain, we have shown that  
 400 the MOST INFLUENTIAL strategy leads to a highly cohesive and polarized group for all  
 401  $k = 1, 2, 3$ , provided the range of the attraction is not too small ( $d_{\text{cut}} > 0.8$  m). For the  
 402 NEAREST strategy, the group is never cohesive for  $k = 1$ , and a much larger range of the  
 403 attraction ( $d_{\text{cut}} > 3.5$  m) is required to ensure the cohesion of the group for  $k = 2$ .

#### 404 Collective motion of larger groups in an unbounded domain

405 For agents moving in an unbounded domain, we have simulated the model with the MOST  
 406 INFLUENTIAL strategy with  $k = 1$ , for groups of  $N = 6$  to 70 individuals starting initially  
 407 in a compact configuration (see Fig. 10C). The group remains highly cohesive for all sizes  
 408 (up to  $N = 70$ ), with a group cohesion of order  $C \sim 0.1$  m. The polarization remains  
 409 high ( $P > 0.7$ ) in groups of size  $N \leq 20$ , and decreases as the group size increases. This  
 410 suggests a smooth cross-over between a schooling phase up to moderate group sizes  
 411  $N \sim 20$ , and a more disordered swarming phase for larger  $N$ . In fact, for the largest  
 412 values of  $N$  investigated, schooling periods are also observed, alternating with periods  
 413 of collective milling, resulting de facto in a reduced polarization of the group. The  
 414 occurrence of the swarming, schooling, and milling phases as a function of the model  
 415 parameters (group size  $N$ , strategy to select the interacting neighbors, intensity and  
 416 range of the attraction/alignment interactions...) will be studied in a future work, as it  
 417 has been previously done for the species *Kuhlia mugil* [32] (a species displaying a smooth  
 418 swimming mode, instead of a burst-and-coast swimming mode).

419 When agents only interact with their nearest neighbor, groups larger than  $N = 5$   
 420 disperse immediately and a larger number of neighbors  $k$  must be taken into account to  
 421 preserve some degree of cohesion. We have also simulated larger groups ( $N = 6, \dots, 26$ ;  
 422  $N$  even) with  $k = 1$  to  $N - 1$  for the NEAREST strategy. The results of S7 Fig (and  
 423 Fig. 10F, in the particular case  $N = 20$ ) show that each agent must interact at least  
 424 with  $k \sim N/2$  nearest neighbors in order to obtain a degree of cohesion similar to the  
 425 one observed for the MOST INFLUENTIAL strategy with  $k = 1$ . Moreover, once  $k > N/2$ ,  
 426 groups become less cohesive as the number of nearest neighbors taken into account by  
 427 agents increases. In fact, for  $N > 6$  and whatever the value of  $k$ , the NEAREST strategy  
 428 always leads to less cohesive groups (S7 FigA) than for the MOST INFLUENTIAL strategy  
 429 with  $k = 1$ , for which  $C \sim 0.1$  m.

430 The simulation results also show that for the NEAREST strategy with  $k < 7$ , the

431 degree of polarization decreases with the group size. Moreover, the polarization reaches  
 432 a maximum for  $k \sim N/2$  until  $N \leq 14$ . For larger groups, interacting with more than  
 433  $k = 7$  nearest neighbors reduces the degree of polarization, which becomes smaller as  $k$   
 434 increases (see S7 FigB and the particular case of  $N = 20$  in Fig. 10F).

### 435 Collective behavior in robotics experiments

436 We now present the results of a series of experiments with  $N = 5$  robots exploiting the  
 437 three interaction strategies considered in the fish model. The robots are programmed  
 438 to reproduce the model behavior (Eqs. (4–15) in Materials and Methods), with model  
 439 parameters adapted to the different spatial and temporal scales of the robotic experi-  
 440 mental setup (see Table 3). In addition, robots operate a control procedure designed to  
 441 resolve collisions with the wall, and most importantly, with other robots (see Materials  
 442 and Methods). Indeed, contrary to point particle agents in the fish model or to real fish  
 443 swimming in shallow water (a truly 3D environment), robots moving on a strictly 2D  
 444 setup cannot physically cross each other. The robots hence combine a behavioral model  
 445 and an engineering-minded control system to deal with real-world physical constraints.  
 446 Our robotic platform provides a concrete implementation of these two elements and  
 447 understanding their interplay and their combined impact on the collective behavior of  
 448 robots is certainly one of the main motivation of the experiments presented here.

449 Panels (DEF) of Figs. 4–8 show the results of the robotic experiments performed in  
 450 the same conditions as those studied with the model, including the case where robots do  
 451 not interact with each other ( $k = 0$ ) and the case where each robot interacts with all its  
 452 neighbors ( $k = 4$ ). However, the robotic experiment for the case  $k = 3$  for the MOST  
 453 INFLUENTIAL strategy was not performed. Counter-milling in robots is illustrated in S6  
 454 Fig, and the density maps of cohesion and polarization are shown in S3 Fig and S4 Fig.  
 455 The robotic platform and the monitoring of a group of 5 robots in motion are shown in  
 456 S2 Video.

457 Despite the fact that the spatial and temporal scales of the robotic platform have  
 458 been scaled at best to correspond to that of the fish experiments (in particular,  $4 \times 4$  cm  
 459 square robots in an arena of radius  $R = 42$  cm vs elongated fish of typical length 3 cm  
 460 swimming in a tank of radius  $R = 25$  cm), the border and other robots have a stronger  
 461 effect on a focal robot at short distance. Indeed, as explained above, the collision  
 462 avoidance protocol (see Materials and Methods) induces effective interactions between  
 463 the robots that have a longer range than the interactions between fish. In addition, the  
 464 square shape of the robot also makes them effectively bigger than if they were elongated  
 465 like fish. Hence, the rescaling of distances as measured in robot experiments is necessary  
 466 to be able to compare the different spatial distributions in fish and robot experiments,  
 467 although it does not affect polarization, counter-milling, or angular distributions. As a  
 468 result, we found a much smaller scaling factor than in model simulations:  $\lambda_R = 0.35$ .  
 469 Note that once the optimal scaling factor is determined, it is kept fixed in all considered  
 470 situations (strategy to select the interacting neighbors and their number  $k$ ). From now,  
 471 all distances in the robot experiments mentioned in this section are hence expressed  
 472 after rescaling to be comparable to corresponding distances in the fish experiments.

473 When  $k = 0$ , robots move independently from each other when they are sufficiently  
 474 far from each other, and tend to remain dispersed along the border of the arena (S5  
 475 Video). The group cohesion is weak (cohesion peaked at  $C \sim 12$  cm; Fig. 4DEF), and  
 476 the distance of the barycenter to the wall is large ( $r_w^B \sim 12$  cm; Fig. 6DEF). Robots are  
 477 relatively more cohesive and closer to the wall compared to the fish model for  $k = 0$  due  
 478 to volume exclusion effects (two colliding robots can end up going in the same direction  
 479 as a result of the control procedure) and because the confining effects of the border of  
 480 the arena are stronger in robots than in agents (see also S3 Fig and S6 Fig). Robots are  
 481 not polarized, as already observed in the fish model simulations for the same condition

482  $k = 0$  (Panels DEF in Figs. 5).

483 Interacting only with  $k = 1$  nearest neighbor does not allow robots to coordinate their  
 484 motion and move as a coherent group (see S6 Video). Panel (D) of Figs. 4–8 (cohesion;  
 485 polarization; distance to the wall; angle with respect to the wall; counter-milling) show  
 486 that the results for  $k = 1$  are similar to those obtained for  $k = 0$ , with a marginal  
 487 improvement of the group cohesion and polarization. On the other hand, when the  
 488 robots interact with their most influential neighbor (S7 Video), the group is highly  
 489 cohesive ( $C \sim 6.5$  cm; Fig. 4F) and highly polarized (large peak at  $P = 1$  in Fig. 5F).  
 490 The robots collectively move close to the border ( $r_w^B \sim 7$  cm; Fig. 6F). Counter-milling is  
 491 also clearly visible (Fig. 8F, S7 Video and S6 Fig). Moreover, for the RANDOM strategy  
 492 with  $k = 1$ , the results are somewhat intermediate between those for the NEAREST and  
 493 MOST INFLUENTIAL strategies, in terms of cohesiveness, polarization, and counter-milling  
 494 (see Panel E in Figs. 4, 5, 8 respectively, and S8 Video). The similarity of the density  
 495 maps of cohesion and polarization with those found in fish experiment is the highest for  
 496 the MOST INFLUENTIAL strategy compared to the other two strategies (S3 Fig and S4  
 497 Fig). Overall, and as confirmed by the Hellinger distances listed in Table 2, the MOST  
 498 INFLUENTIAL strategy with  $k = 1$  produces highly cohesive and polarized robot groups  
 499 leading to a qualitative agreement with fish experiments, whereas the NEAREST strategy  
 500 does not even lead to any significant group coordination.

501 Extending the interaction to the  $k = 2$  nearest neighbors reinforces group coordination  
 502 (S9 Video): groups are more cohesive (the peak in the PDF of  $C$  decreases from around  
 503 10 cm for  $k = 1$ , to 7 cm), and simultaneously more polarized (S3 Fig). However, the  
 504 polarization remains weak compared to fish experiments, and even compared to the  
 505 MOST INFLUENTIAL strategy for  $k = 1$ : the PDF of  $P$  has a wide region of high values  
 506 centered in  $P \approx 0.85$  and is not peaked at  $P = 1$  (Fig. 5D). The high peak at  $P = 0.6$   
 507 reveals that situations in which groups of 4 robots move in the same direction while the  
 508 fifth robot moves in the opposite direction are quite frequent. Wide groups ( $C > 8$  cm,  
 509 Fig. 4D) moving far from the border ( $r_w^B > 9$  cm, Fig. 6D) are still frequent, and  
 510 counter-milling is still barely visible (S6 Fig). On the other hand, interacting with the  
 511 two most influential neighbors definitively produces patterns that are similar to those  
 512 observed in fish experiments, especially if we consider the polarization, where the peak  
 513 at  $P = 1$  clearly narrows and doubles its height (Fig. 5F and S10 Video), although the  
 514 improvement with respect to the MOST INFLUENTIAL strategy with  $k = 1$  is small, or  
 515 even negligible, if we consider the counter-milling index (Fig. 8F). Again, the RANDOM  
 516 strategy with  $k = 2$  leads to an overall much better agreement with fish experiments  
 517 than the NEAREST strategy with  $k = 2$  (see Hellinger distances between PDF in Table 2).  
 518 Except for the weaker polarization, the results for the RANDOM strategy are similar to  
 519 the ones obtained for the MOST INFLUENTIAL strategy with  $k = 2$  (see Table 2 and S11  
 520 Video).

521 For  $k = 3$ , the results for the NEAREST strategy (see S12 Video) improve drastically  
 522 and are in comparable agreement with fish experiments as the results for the RANDOM  
 523 strategy (S13 Video), and on par with those for the MOST INFLUENTIAL strategy for  
 524  $k = 1, 2$  (see Table 2). For the NEAREST and RANDOM strategies (sharing 2, and often  
 525 3, common neighbors for  $k = 3$ ), groups are highly cohesive (Fig. 4DE) and polarized  
 526 (Fig. 5DE), with a narrower PDF of  $C$  than in fish experiments, pointing to the robot  
 527 groups having less internal fluctuations than fish groups. Accordingly, the PDF of  $r_w^B$   
 528 (Fig. 6DE) is peaked at the same value as in fish experiments,  $r_w^B \approx 5.5$  cm, but is again  
 529 narrower, with much less weight at distances  $r_w^B > 8$  cm. The PDF of  $\theta_w^B$  (Fig. 6DE) is in  
 530 good agreement with fish experiments, and counter-milling is clearly obtained (S6 Fig).  
 531 When robots interact with  $k = 4$  neighbors (S14 Video), the results are very similar to  
 532 the case  $k = 3$  within the non negligible statistical fluctuations due to our shorter robot  
 533 experiments compared to the fish experiments and fish model simulations.

534 In conclusion, many of the results of the robotic experiments are qualitatively similar  
 535 to those found in the simulations of the model, despite the robots being submitted  
 536 to real-world physical constraints. Yet, for robots, the MOST INFLUENTIAL strategy  
 537 with  $k = 1$  is found to lead to cohesive and polarized groups (like in the model), while  
 538 the NEAREST strategy with  $k = 1$  does not lead to any significant group coordination  
 539 (weaker coordination for the model in a confining domain, but no cohesive groups in an  
 540 unbounded domain).

## 541 Discussion

542 Collective motion involving the coherent movements of groups of individuals is primarily  
 543 a coordination problem. Each individual within a group must precisely adjust its  
 544 behavior to that of its neighbors in order to produce coordinated motion. Determining  
 545 how these relevant neighbors are selected at the individual scale is therefore a key  
 546 element to understand the coordination mechanisms in moving animal groups. Previous  
 547 experimental works on fish and birds have identified interacting neighbors using short-  
 548 term directional correlations [17,34] or anisotropy of the position of the nearest neighbors  
 549 [21]. In a starling flocks (*Sturnus vulgaris*), each bird coordinates its motion with a finite  
 550 number of closest neighbors (typically seven), irrespective of their distance [21]. However,  
 551 in fish schools, experimental studies suggest that each individual only interacts with a  
 552 smaller number of influential neighbors. For instance, in the mosquitofish (*Gambusia*  
 553 *holbrooki*), each fish mostly interacts with a single nearest neighbor [35]. In the rummy  
 554 nose tetra (*Hemigrammus rhodostomus*) during collective U-turns [28,36], the analysis  
 555 of directional correlations between fish suggests that each fish mainly reacts to one or  
 556 two neighbors at a time [28]. These results are in line with theoretical works that have  
 557 suggested that, instead of averaging the contributions of a large number of neighbors,  
 558 as suggested by many models [18–20,23,37,38], individuals could pay attention to only  
 559 a small number of neighbors [25–28,39]. This mechanism would overcome the natural  
 560 cognitive limitation of the amount of information that each individual can handle [33].

561 Here, we addressed this question in groups of five *H. rhodostomus* swimming in a  
 562 circular tank. This species of fish is of particular interest because of its tendency to form  
 563 highly polarized groups and its burst-and-coast swimming mode [14], which allows us to  
 564 consider that each fish adjusts its heading direction at the onset of each bursting phase,  
 565 that is labeled as a “kick”. Just before these brief accelerations, a fish integrates and  
 566 filters the information coming from its environment and picks its resulting new heading.

567 In our experiments, groups of five fish remain highly cohesive, almost perfectly  
 568 polarized, and swim along and close to the wall of the tank, keeping the same direction of  
 569 rotation for very long periods [36]. Fish groups also display a remarkable counter-milling  
 570 collective behavior where individual fish rotate around the group barycenter in the  
 571 opposite direction to that of the group in the tank, so that individuals alternate their  
 572 positions at the front of the group.

573 Based on a previous work in which we have reconstructed and modeled the form of the  
 574 interactions of *H. rhodostomus* fish swimming in pairs [14], we analyzed three strategies  
 575 for combining the pairwise interactions between a focal fish and a number  $k = 1$  to 3 of  
 576 its neighbors by means of a computational model and a robotic platform. In the NEAREST  
 577 strategy, neighbors are selected according to their distance to the focal individual. In  
 578 the RANDOM strategy, neighbors are randomly chosen, and in the MOST INFLUENTIAL  
 579 strategy, neighbors are selected according to the intensity of their contribution to the  
 580 heading variation of the focal individual. The impact of these strategies on the resulting  
 581 collective behavior was then measured and analyzed by means of five quantities: group  
 582 cohesion, group polarization, distance and relative orientation of the barycenter with  
 583 respect to the border of the tank, and counter-milling index.

584 Our results suggest that when individuals (agents or robots) interact with a minimal  
 585 number of neighbors, namely two, a group of individuals is able to reproduce the main  
 586 characteristics of the collective movements observed in the fish experiments.

587 In the simulations of the model for  $N = 5$ , when the agents are interacting with  
 588 a single neighbor, this immediately leads to the formation of groups. Whatever the  
 589 strategy used to select a neighbor, the quantities used to quantify group behavior show  
 590 that the exchange of information with a single neighbor leads agents to get closer to each  
 591 other, at least temporarily for the NEAREST strategy. However, whatever the strategy  
 592 considered, cohesion, polarization, and counter-milling are still weak compared to fish  
 593 experiments, although the MOST INFLUENTIAL strategy convincingly leads to the best  
 594 group coordination for  $k = 1$ .

595 The simulations of the model in an unbounded domain show that group cohesion is  
 596 maintained over long periods of time when agents only interact with their most influential  
 597 neighbor, provided the attraction range is above a critical threshold distance. However,  
 598 when agents only interact with their nearest neighbor, this systematically leads to the  
 599 diffusive dispersion of the group. For groups of size up to  $N = 70$ , interacting with the  
 600 most influential neighbor leads to compact groups, while one needs to consider typically  
 601 at least  $\sim N/2$  nearest neighbors to achieve the same result for the NEAREST strategy.  
 602 Therefore, the cohesion of the group observed in the arena is not a merely consequence  
 603 of the confinement of the agents, but mainly results from the higher quality of the  
 604 information provided by the influential neighbors in comparison to the one provided by  
 605 the nearest neighbors.

606 Then, when agents acquire more information about their environment ( $k = 2$ ), all  
 607 the interaction strategies implemented in the model give rise to collective behaviors that  
 608 are in qualitative agreement with those observed in the experiments with fish, and a  
 609 quantitative agreement is even reached for some quantities characterizing group behavior  
 610 (see Table 1). When agents collect even more information about their environment  
 611 (*i.e.*, when they pay attention to  $k = 3$  neighbors), the agreement with fish experiments  
 612 is not improved if the neighbors are chosen according to their influence. However,  
 613 groups become more cohesive and polarized when the agents interact with their nearest  
 614 neighbors. Yet, for  $k = 3$ , the three strategies lead to comparable results, which is  
 615 consistent with the facts that two strategies have necessarily at least two common  
 616 neighbors for groups of five individuals. Note that for  $k = 2$  and  $k = 3$ , and for all  
 617 three strategies, the intensity of the counter-milling is larger in the model than in fish  
 618 experiments, suggesting that the internal structure of real fish groups is more rigid than  
 619 predicted by the model.

620 In summary, the simulation results clearly indicate that group behaviors similar  
 621 to those observed in fish experiments can be reproduced by our model, provided that  
 622 individuals interact with at least two of their neighbors at each decision time and no  
 623 clear gain is obtained when agents interact with a third additional neighbor. When only  
 624 one interacting neighbor is considered, the MOST INFLUENTIAL strategy leads to the  
 625 best group coordination, which even survives when the group moves in an unbounded  
 626 domain.

627 By implementing the behavioral fish model and the same local interaction strategies  
 628 in our robotic platform, we also investigated the impact of the physical constraints and  
 629 the collision avoidance protocol based on speed control on the group behavior. The  
 630 MOST INFLUENTIAL strategy is much more efficient than the two other strategies to  
 631 ensure group cohesion and polarization (see Table 2). Remarkably, and as already  
 632 observed in the model simulations, even when robots only interact with their most  
 633 influential neighbor, the group remains highly cohesive and polarized, and close to the  
 634 border. By contrast, when robots only interact with their nearest neighbor, they are  
 635 not able to exhibit any kind of coordinated behavior. Everything happens as if pairwise

636 interactions between robots were screened by the effect induced by the collision avoidance  
637 protocol: the distributions of the group cohesion, the polarization, and the distance  
638 of the barycenter of the group to the border of the tank are almost identical to those  
639 obtained with the null model, in which no interaction exists between robots except for  
640 collision avoidance. When robots interact with two neighbors, the agreement with the  
641 results of fish experiments is improved, but it is only when robots interact with three  
642 nearest neighbors that the NEAREST strategy produces highly cohesive and polarized  
643 groups.

644 Overall, and even more convincingly than in the case of the fish model, the MOST  
645 INFLUENTIAL strategy leads to the best overall agreement with fish experiments for  $k = 1$   
646 and  $k = 2$ , even producing strongly coordinated groups for  $k = 1$ . Compared to the  
647 case of the fish model, the NEAREST strategy does not lead to any significant group  
648 coordination for  $k = 1$ , and only to moderately cohesive and polarized groups for  $k = 2$ ,  
649 yet being even less efficient than the RANDOM strategy. The robot collision avoidance  
650 protocol induces a strong effective repulsion between close neighbors, which screens the  
651 behavioral interactions for the strategy based on these nearest neighbors.

652 Note that implementing the  $k$ -MOST INFLUENTIAL strategy in a computational  
653 model for larger groups of agents is not more computationally challenging than the  
654 implementation of the more common  $k$ -NEAREST strategy, and is even less demanding  
655 than the consideration of the first layer of neighbors in a Voronoi construction used in  
656 many phenomenological flocking models [21, 22, 32]. For very large groups ( $N > 10000$ ),  
657 rarely considered in the context of fish models, the implementation of the  $k$ -MOST  
658 INFLUENTIAL and  $k$ -NEAREST strategies could also be optimized by exploiting grid  
659 algorithms commonly used in computational physics and astrophysics.

660 However, beyond its purely computational complexity, the possible biological relevance  
661 of the MOST INFLUENTIAL strategy (with small  $k$ ) for fish and potentially other animals  
662 is certainly an important question. In vertebrates, and in particular in fish, the midbrain  
663 and forebrain networks are carrying out computation in parallel to process the visual  
664 information and select the most salient stimuli that are the focus of attention. The  
665 midbrain network continuously monitors the environment for behaviorally relevant  
666 stimuli [40]. This is a primary site where the information about the neighbors is filtered  
667 for cognitive decision. Then, the forebrain network selects those stimuli on which the fish  
668 focuses its attention. The interaction strategies that we have investigated in this work  
669 correspond to different ways for an individual to focus its attention on the stimuli (*i.e.*,  
670 its relevant neighbors). In the context of fish schools, individuals filter the information  
671 from their environment and thus limit their attention to a small set of their most salient  
672 neighbors [25–27], hence giving priority to the few neighbors to be avoided (by moving  
673 away or by aligning their headings) or the ones to be followed. These few neighbors  
674 requiring an immediate action from the focal fish should, by definition, trigger a larger  
675 response than other neighbors, hence making the notion of most influential neighbors  
676 quite natural. Our results show that each fish interacts with typically two neighbors  
677 that are the most salient, a process which reduces the amount of information that needs  
678 attention and which hence permits to avoid any cognitive overload.

679 In conclusion, each individual must acquire a minimal amount of information about  
680 the behavior of its neighbors for coordination to emerge at the group level, thus allowing  
681 fish to avoid information overload when they move in large groups [33].

682 **Materials and Methods**

683 **Fish experiments**

684 **Ethics statement.** Our fish experiments have been approved by the Ethics Committee  
 685 for Animal Experimentation of the Toulouse Research Federation in Biology N° 1 and  
 686 comply with the European legislation for animal welfare.

687 **Study species.** Rummy-nose tetras (*Hemigrammus rhodostomus*) were purchased  
 688 from Amazonie Labège (<http://www.amazonie.com>) in Toulouse, France. Fish were kept  
 689 in 150l aquariums on a 12:12 hour, dark:light photoperiod, at 25.2 °C ( $\pm 0.7$  °C) and  
 690 were fed *ad libitum* with fish flakes. The average body length of the fish used in these  
 691 experiments is 31 mm ( $\pm 2.5$  mm).

692 **Experimental setup.** We used a rectangular experimental tank of size 120 × 120 cm,  
 693 made of glass, supported by a structure of metal beam 20 cm high. A plywood plate  
 694 was interposed between the mesh and the basin to dampen the forces exerted on the  
 695 glass basin by its own weight and water. This structure also enables the attenuation  
 696 of vibrations. The setup was placed in a chamber made by four opaque white curtains  
 697 surrounded by four LED light panels to provide an isotropic lighting. A circular tank of  
 698 radius  $R = 250$  mm was set inside the experimental tank filled with 7 cm of water of  
 699 controlled quality (50% of water purified by reverse osmosis and 50% of water treated  
 700 by activated carbon) heated at 24.9 °C ( $\pm 0.8$  °C). Reflection of light due to the bottom  
 701 of the experimental tank is avoided thanks to a white PVC layer.

702 Each trial started by placing groups of  $N = 5$  fish randomly sampled from the  
 703 breeding tank into the circular tank. Fish were let for 10 minutes to habituate before  
 704 the start of the trial. A trial then consisted of one hour of fish freely swimming in  
 705 the circular tank with experimenters out of the room. Fish trajectories were recorded  
 706 by a Sony HandyCam HD camera filming from above the setup at 25 Hz (25 frames  
 707 per second) in HDTV resolution (1920×1080p). We performed 11 trials with groups of  
 708  $N = 5$  fish, and for each trial, we used different fish taken from the breeding tank.

709 **Robotic platform**

710 **Robots.** We used a robotic platform composed by small compact mobile robots that  
 711 we named “Cuboids”, a name chosen in reference to the first realistic computer program  
 712 that simulated the flocking behavior in birds and the schooling behavior in fish, called  
 713 “Boids”, developed in 1986 by Craig Reynolds [41]. The Cuboids robots were specifically  
 714 designed by us for this experiment.

715 Cuboids have a square basis of 40 × 40 mm, they are 60 mm high and weigh 50 g  
 716 (Fig. 11). We now describe the elements of a Cuboid (numbers between parentheses  
 717 refer to labels in Fig. 11). Each robot is equipped with two differential wheels (7)  
 718 driven by small DC motors (13). The small belts (9) connect wheels to the DC motors,  
 719 which can drive the robot with a maximum speed of 50 mm/s. The two wheels are  
 720 mounted on a central axis (6). An IEEE 802.11n/WIFI module (8) with a range of  
 721 approximately 200 m is used for communication network between robot and a wireless  
 722 router. A Li-Poly rechargeable battery (15) provided energy for about 6 hours in our  
 723 experimental conditions. In addition, a coil (12) located under the robot, can be used  
 724 to charge the robot wirelessly while it is working. The charging circuit is located on  
 725 the side board (11). The robot bottom hosts a 32-bit, 168 MHz ARM microprocessor  
 726 STM32F4 (14), which can provide multi control loops with the time duration up to  
 727 2 ms. Besides, another 8-bit microcontroller PIC18F25k22 is mounted on the top sensor  
 728 board (1), which controls a LCD screen (16) to display information and a 3-colors

729 LED (17). The microprocessor communicates with the microcontroller by 4 copper  
 730 bars (4), which can simultaneously provide power and communication bus.

731 Each Cuboid also has several sensors to measure the relative positions of other robots  
 732 in its neighborhood and to send and receive messages from these robots. Within a  
 733 sensing range of about 20 cm, a robot can send messages (infrared signals) by the center  
 734 IR transmitter (3). There are two IR receivers (2) on both sides of the robots, which  
 735 can determine the distance of a neighboring robot that transmits the infrared signal.  
 736 From the two distance values provided by the IR receivers, the angle with which this  
 737 neighboring robot is perceived by the focal robot can be calculated by triangulation.  
 738 Furthermore, the relative position of the neighboring robot to the focal one can be  
 739 computed by the information of the distance and the angle of perception acquired before.  
 740 On the other side, the IR signal also carries a short message that includes information  
 741 on robot ID, orientation angle, speed and states. The heading of a Cuboid is measured  
 742 by a motion tracking sensor MPU-9250 (18). This device consists of a 3-Axis gyroscope,  
 743 a 3-Axis accelerometer, and a 3-Axis magnetometer. Hence, the MPU-9250 is a 9-axis  
 744 Motion Tracking device that also combines a Digital Motion Processor. With its I2C bus  
 745 connected with PIC18F25K22, the MPU-9250 can directly provide complete 9-axis  
 746 Motion Fusion output to the microcontroller. These sensing and local communication  
 747 devices have not been used in the experiments that have been done in a supervised  
 748 mode.

749 We tested the model with the robotic platform because there are many physical aspects  
 750 that have to be considered to assess the robustness of the coordination mechanisms when  
 751 they are implemented in a physical hardware. These physical aspects include the friction  
 752 of wheels, the noise of gear box, the blurring of the camera, the wrong identification of  
 753 the tracker, the delay of the communication, the overload of computation, the blocking  
 754 of the onboard communication bus, the square shape collision of the robot frame, the  
 755 mismatch parameters of the interaction model, the impact of the obstacle avoidance  
 756 protocol, and the non-holonomic constraint of the robot. All these physical aspects can  
 757 have a large effect on the individual and collective behaviors (especially when robots  
 758 move in a crowded space) and are difficult to include in a model.

759 **Experimental platform.** The robotic experimental setup consisted of a circular  
 760 arena of radius 420 mm resting on a  $1 \times 1$  m square flat surface with a camera (Basler  
 761 piA2400-17gc) mounted on the top (see Fig. 12). The setup was placed in a chamber  
 762 made by 3 opaque wooden boards and 1 white curtain. 2 LED light panels provide a  
 763 diffused lighting. A circular cardboard wall of radius  $R = 420$  mm delimited the border  
 764 of experimental platform. The floor of the experimental platform was made with a rough  
 765 wooden board that prevented the reflections of light. A computer is connected to the  
 766 camera to supervise the actions of the robots in the arena, and to perform the necessary  
 767 image processing to track each robot and compute in real time its position  $(x, y)$  and  
 768 heading angle  $\phi$ .

769 The clock cycle of the imaging process module is 300 ms, a limit imposed by the  
 770 camera updating speed. A tracking software (Robots ID Tracker), based on the Kalman  
 771 filter technology, is then used to assign the location data to the right robots on a shorter  
 772 time scale (every 20 ms). These data are used in real time to control the reaction of  
 773 each robot in its changing environment, and are also stored in the computer for off-line  
 774 *a posteriori* trajectory analysis. Thanks to the high precision of our tracking system, we  
 775 are able to compute in real time and for each robot  $i$  the quantities that characterize its  
 776 instantaneous state with respect to its environment: the distance and relative orientation  
 777 to the wall  $r_w^i$  and  $\theta_w^i$ , and the distance, relative angular position, and relative orientation  
 778 with respect to other robots  $j$ ,  $d_{ij}$ ,  $\psi_{ij}$  and  $\phi_{ij}$ , respectively (Fig. 2). All this information  
 779 is used to compute the output of the interactions of a robot with its local environment

780 by means of an Object-Oriented Programming software developed by us. The robot  
 781 behavior is driven by the mathematical fish model, which combines the interactions with  
 782 the obstacles and with the other robots, and generates the control signals dispatched  
 783 in a distributed way to each individual robot through a WIFI communication router  
 784 (HUAWEI WS831).

785 Although the robot has its own sensors to ensure it autonomous control and move-  
 786 ments, in this work, we used a remote-control mode. This is because our goal was to  
 787 compare the performances between the software simulation and the robot experiment  
 788 with the same computational model and the same local information input (see the  
 789 Hardware In Loop simulation in Fig. 13; [42]).

790 Fig. 13 (red and blue boxes) shows the “Hardware In Loop” (HIL) simulation used  
 791 to control the Cuboids robots. The HIL simulation integrates the robots hardware into  
 792 the distributed control loops of the platform computer software. As such, it differs  
 793 from a traditional software simulation, being a semi-real one. Compared with pure  
 794 theoretical simulations “in silico” (*i.e.*, the software simulation box in Fig. 13), the HIL  
 795 simulation integrates both the hardware constraints (*i.e.*, the mechanical constraints of  
 796 the robots, the time delay of the control loop which includes the shooting by the camera,  
 797 the time of calculation and sending orders by the WIFI router), and those that result  
 798 from the movement of the robots in a physical environment, in particular the need to  
 799 avoid collisions with obstacles and other robots (see the blue box in Fig. 13).

800 The main difference between the HIL simulation and the software simulation is the  
 801 real time control of the behavior of each robot, which is achieved by the *Motion Control*  
 802 and the *Real Time Control* modules (see the red box in Fig. 13).

803 The Motion Control module can produce two kinds of motion patterns: rotating and  
 804 moving straight. The first motion pattern is *Spot Rotation*, which means that the robot  
 805 rotates around its center by means of wheels differential driving. The speed control of  
 806 the two wheels is described by the following equation:

$$V_{R,i} = -V_{L,i} = p_t \delta\phi_{ci},$$

807 where  $V_{R,i}$  and  $V_{L,i}$  are the speeds of the right and left wheels of the robot respectively,  
 808  $p_t$  is a constant factor of proportionality, and  $\delta\phi_{ci}$  is the real-time value of the heading  
 809 variation, which is determined by the Real Time Control module. The second motion  
 810 pattern that the robot can display is *Moving Straight*, where the speeds of the left and  
 811 right wheels are the same:

$$V_{R,i} = V_{L,i} = p_m l_{ci},$$

812 where  $p_m$  is a constant factor of proportionality and  $l_{ci}$  is the value of the kick length,  
 813 which is also determined by the Real Time Control module.

814 The Real Time Control module ensures the safe movement of each robot and helps  
 815 the robot to rotate and move straight towards a target place. This module first converts  
 816 the decision of the computational model ( $\delta\phi_i(t_{dec}), l_i(t_{dec})$ ) at the last decision time  $t_{dec}$   
 817 into a real-time decision that is then performed by the robot, ( $\delta\phi_{ci}(t), l_{ci}(t)$ ),  $t > t_{dec}$ .

818

---



---

### Algorithm of the Real Time Control module

---

820

821  
 822 **Input :**

823     Computational Model decision: ( $\delta\phi_i(t_{dec}), l_i(t_{dec})$ ),

824     Current position and heading: ( $x_{ci}(t), y_{ci}(t)$ ),  $\phi_{ci}(t)$ .

825 **Output :**

826     Real-time decision: ( $\delta\phi_{ci}(t_{dec}), l_{ci}(t_{dec})$ )

```

827     1.  $\delta\phi_{ci}(t) = \phi_i(t_{dec}) + \delta\phi_i(t_{dec}) - \phi_{ci}(t), t > t_{dec}$ .
828     2.  $l_{ci}(t) = l_i(t_{dec}) - \sqrt{(x_{ci}(t) - x_i(t_{dec}))^2 + (y_{ci}(t) - y_i(t_{dec}))^2}$ .
829     3. If  $|\delta\phi_{ci}(t)| > \delta\phi_{Threshold}$ , then
830         Do Spot rotation for Motion Control in real-time.
831     else
832         Do Moving straight for Motion Control in real-time.
833     4. If  $|\delta\phi_{ci}(t)| < \delta\phi_{Threshold}$  and  $l_{ci}(t) < l_{Threshold}$ , then
834         the target is reached;
835         Goto Compute state (computational model) for a new decision.
836     5. If the path is not free, then
837         Do Obstacle Avoidance procedure.
838     6. End

```

---

841 There are two time-scales in the control for the robots. The long time scale is  
842 determined by the time taken in simulating the computational model, which is about  
843 1.3 s. The short time-scale corresponds to the Real Time Control module, which operates  
844 at a high frequency with respect to the real time motion of the robot. This module is  
845 used to control the navigation of the robot toward the target and the obstacle avoidance  
846 (see the table of Algorithm of the Real Time Control module). The maximum time  
847 interval of the Real Time Control module is 20 ms for each robot. With such a fast  
848 frequency, the communication channel is always busy. To solve this problem, we designed  
849 and used a specific protocol to broadcast in one loop the Motion Control command ( $V_{R,i}$ ,  
850  $V_{L,i}$ ) to each respective robot  $i$ , based on TCP protocol, thus guaranteeing the speed  
851 and the robustness of the communication channel. The average duration of one of these  
852 loops (for all robots) in the Real Time Control is about 13 ms (Fig. 13).

853 **Implementation of the behavioral model in the robots.** We use the LabVIEW  
854 object-oriented programming (OOP) tool to design the distributed control software  
855 for the Cuboids robots (Fig. 13). It first establishes independent memories for each  
856 robot as an agent to store real time information, such as robot ID, location and heading  
857 ( $x_{ci}(t), y_{ci}(t), \phi_{ci}(t)$ ) at time  $t$ , and real time decision ( $\delta\phi_{ci}(t), l_{ci}(t)$ ). We design a state  
858 machine control structure to implement the HIL simulation control for each robot. With  
859 the new speed control command determined by the *Motion Control* module, the actuators  
860 of the robot are controlled wirelessly by the WIFI signals sent by the computer. The  
861 robot controls its wheels to move towards the new target place while LED colors display  
862 the state of the robot.

863 Robots use a constant kick length  $l_i(t_{dec})$  of around 8 cm, that is, twice the body  
864 length of a robot, which corresponds to the mean kick length measured in experiments  
865 with five fish. Using a constant straight step also allows to check if the new target  
866 place can be reached or not, in particular, to prevent the case where the agent could be  
867 intercepted by another agent, in which case the distance traveled by the agent will be  
868 shorter than  $l_i(t_{dec})$ .

869 The state machine control structure for an individual robot includes two main states:  
870 COMPUTE state and MOVE state; see the flow chart of the robot state machine and  
871 the finite state machine diagram in Fig. 14 and S8 Fig respectively. The robots are  
872 programmed to perform a burst-and-coast movement mimicking the swimming mode of  
873 fish. When a robot is in the COMPUTE state at time  $t_{dec}$ , the computational model  
874 determines a new decision ( $\delta\phi_i(t_{dec}), l_i(t_{dec})$ ) (see hereafter and [14] for the description

875 of the model; the model parameter for the robots are listed in 3 Table). After that, the  
 876 robot switches to the MOVE state and adjusts its wheels to move towards the decision  
 877 place in real time thanks to the *Motion Control* and *Real Time Control* modules. Since  
 878 other robots are moving around asynchronously, the robot must avoid these dynamic  
 879 obstacles while being in the MOVE state. To prevent collisions between robots, we  
 880 designed and implemented an obstacle avoidance protocol. When no valid targets can  
 881 be generated during the COMPUTE state (due to the impediment imposed by nearby  
 882 robots), the robot generates a valid target place by means of a scanning method and,  
 883 alternatively, just moves back over a short distance. However, this circumstance rarely  
 884 occurs in our experiments (except in the absence of behavioral interactions,  $k = 0$ ; see  
 885 S5 Video).

886 We describe below the two states and the additional procedures used to avoid collisions  
 887 with dynamical obstacles.

- 888 • COMPUTE State: This state generates a new decision  $(\delta\phi_i(t_{dec}), l_i(t_{dec}))$  for  
 889 the focal robot by means of the computational model, which is programmed in  
 890 MATLAB. In this state, the robot takes the information about its local environment  
 891  $(r_{w,i}, \theta_{w,i})$  and selects the neighbors to be taken into account corresponding to the  
 892 current local interaction strategy. Then, the robot computes the variation of its  
 893 heading angle  $\delta\phi_i(t_{dec})$  that, combined with the kick length  $l_i(t_{dec})$ , determines a  
 894 new target place. The location of the new target is then checked and validated  
 895 by the OOP software so as to avoid any collision with static obstacles, before the  
 896 robot switches to the MOVE state (see Fig. 14, S8 Fig). While a robot is in the  
 897 COMPUTE State, the white LED light is turned on.
- 898 • MOVE State: In this state the robot evaluates whether its heading angle  $\phi_{ci}$  is  
 899 aligned with the new pace target. If the deviation  $\delta\phi_{ci}$  is too large, the robot  
 900 first rotates towards the target and then moves straight until it reaches the target,  
 901 thanks to the *Motion Control* module. Then, when the robot successfully reaches  
 902 the target, it returns to the COMPUTE state to determine a new target. While a  
 903 robot is in the MOVE State, the green LED light is turned on.
- 904 • Obstacle Avoidance Protocol: This procedure is triggered as soon as the target  
 905 path of the focal robot  $i$  crosses the safety zone of another robot  $j$ . The safety  
 906 zone is a circular area around a robot of diameter of 80 mm. In this case, the  
 907 focal robot  $i$  first stops and computes whether it can continue moving or not,  
 908 according to the information it has about the distance  $d_{ij}$  and relative angular  
 909 position  $\psi_{ij}$  of the neighboring robot. If the focal robot has the moving priority  
 910 (determined by a large value of the angle of perception,  $|\psi_{ij}| > 90^\circ$ , meaning that  
 911 the robot is a temporary leader [14]), or if the distance is larger than the diameter  
 912 of the circle of security ( $d_{ij} > 80$  mm, meaning that the robot  $j$  is far enough),  
 913 the moving condition is satisfied and the focal robot  $i$  successfully switches back  
 914 into the MOVE state. If not, it repeatedly checks the values  $d_{ij}$  and  $\psi_{ij}$  until the  
 915 moving condition is satisfied. If the focal robot cannot go back into the MOVE  
 916 state within 3 seconds, it toggles to the COMPUTE state to determine a new  
 917 target.
- 918 • No Valid Target Procedure: This procedure is triggered when the robot is in the  
 919 COMPUTE state and cannot generate a valid target place within 3 seconds. In  
 920 this situation, the robot scans the local environment from its front to the nearest  
 921 neighbor located at one of its sides. If there exists a free space for generating a  
 922 target place, the robot toggles to the MOVE state. If, after scanning, no free space  
 923 is available for moving, the robot moves back over a predefined distance of 80 mm  
 924 (approximately two robot body lengths) and then toggles to the COMPUTE state  
 925 to determine a new target place.

926 In the robotic experiments, we performed one experiment for each combination of  
 927 interactions with about 8000 kicks in average for all the 5 robots. The duration time of  
 928 experiments performed for each condition was the following:

- 929 • Interacting with  $k = 1, 2$  and 3 nearest neighbors: 61, 62 and 63 min respectively.
- 930 • Interacting with  $k = 1, 2$  and 3 randomly chosen neighbors: 65, 128 and 48 min  
 931 respectively.
- 932 • Interacting with  $k = 1$  and 2 most influential neighbors: 68 and 82 min respectively.
- 933 • Interacting with  $k = 0$  and  $k = 4$  neighbors: 150 min in both cases.

### 934 Data extraction and preprocessing

935 Fish data were extracted from videos recorded during 11 sessions along 11 days in 2013,  
 936 by means of idTracker software version 2.1 [43], producing 11 data files with the position  
 937 (in pixels) of each fish in each frame, with a time step of  $\Delta t = 0.04$  s (corresponding  
 938 to images taken with a frequency of 25 fps). Data were located in a rectangle of size  
 939  $[471.23, 1478.48] \times [47.949, 1002.68]$  containing the circular tank of diameter 50 cm. The  
 940 conversion factor from pixels to meters is  $0.53 \times 10^{-3}$  m/pix. The origin of coordinates  
 941  $T(0, 0)$  is set to the center of the tank (Fig. 1).

942 We found that trajectory tracking was satisfactorily accurate. However, fish were  
 943 often misidentified, making impossible the direct use of the data provided by the tracking  
 944 system. We thus implemented a procedure of identity reassignment that provided us  
 945 with the proper individual trajectories. In short, the procedure is a sorting algorithm  
 946 where fish identities are successively reassigned in such a way that the coordinates of  
 947 each fish at the next time step are the closest ones to the coordinates they had at the  
 948 previous time. That is, the fish  $i$  at time  $t$  is assigned the coordinates of fish  $j$  at time  
 949  $t + \Delta t$  that minimize the distance covered by the 5 fish.

950 Data were then grouped in a single file, counting 1.077.300 times, *i.e.*, almost 12 hours  
 951 where the position of each fish is known. Then, times where at least one fish freezes  
 952 were removed. Fish often remain stationary. We considered that a fish is at rest when  
 953 the distance covered in 60 frames is smaller than 30 pixels, that is, when the mean speed  
 954 is smaller than 6.6 mm/s during at least 2.4 seconds. We discarded more than half of  
 955 the data using this procedure (around 5.5 hours of data remaining). We then extracted  
 956 the continuous sequences lasting at least 20 seconds, obtaining 293 sequences for a total  
 957 duration of around 3h 10mn.

958 Fish trajectories were then segmented according to the burst-and-coast typical  
 959 behavior of this species [14] (see Fig. 1C). We used a time window of 0.2 s to find the  
 960 local minima of the velocity. These points are used to define the onset of a kick event.  
 961 We detected 60312 kicks, which means that a fish makes in average around 1 kick/s.

962 In [14], no statistically meaningful left/right asymmetry in the trajectories of single  
 963 fish ( $\sim 300000$  kicks recorded) or pairs of fish ( $\sim 200000$  kicks recorded) was observed.  
 964 Hence, for any observed trajectory, the mirror trajectory (that is the same one, but  
 965 as observed from the bottom of the tank instead of from the top) would have exactly  
 966 the same probability to be observed. Assuming the absence of left/right asymmetry for  
 967 groups of 5 fish (as observed for 1 and 2 fish), leads to the same conclusion. Groups  
 968 of 5 fish (as well as groups of 5 model fish or 5 robots) rotate clockwise (CW) or  
 969 counter-clockwise (CCW) around the center of the tank for long periods (collective  
 970 U-turns in groups of 2-20 fish have been studied in [36]). Therefore, for the much shorter  
 971 present fish (and especially robots) experiments compared to [14] (60312 recorded kicks,  
 972 instead of  $\sim 500000$ ), one would observe an artificial asymmetry (groups turning more  
 973 often CW than CCW, or the opposite) only due to the lack of statistical sampling of the

974 rare collective direction changes. In order to avoid this artificial asymmetry, for each  
 975 set of 5 trajectories (fish and robots), we have added the mirror set (the trajectories  
 976 as seen from the bottom of the tank). Again, this procedure is perfectly sound once  
 977 the absence of left/right asymmetry observed in very long 1- and 2-fish experiments is  
 978 reasonably assumed to hold in our present 5-fish experiments (the model and its version  
 979 implemented in robots have obviously no left/right asymmetry, per construction). Note  
 980 that only the distribution of  $\theta_w^B$  is affected by this symmetrization procedure, and not  
 981 the distributions of group cohesion, polarization, distance to the wall, counter-milling  
 982 index (the latter being a relative quantity), which are invariant by the mirror symmetry.

983 To calculate the heading angle of a fish at time  $t$ , we considered that the direction  
 984 of motion is well approximated by the velocity vector of the fish at that time  $t$ . The  
 985 heading angle  $\phi(t)$  of a fish is thus given by the angle that its velocity  $\vec{v} = (v_x, v_y)$  makes  
 986 with the horizontal line, that is,

$$\phi(t) = \text{ATAN2}(v_y(t), v_x(t)). \tag{1}$$

987 Positive angles are measured in counter-clockwise direction and ATAN2 returns a value in  
 988  $(-\pi, \pi]$ . The components of the velocity are estimated with backward finite differences,  
 989 *i.e.*,  $v_x(t) = (x(t) - x(t - \Delta t))/\Delta t$  and  $v_y(t) = (y(t) - y(t - \Delta t))/\Delta t$ .

990 The robot trajectories were extracted with a custom-made tracking software based  
 991 on Kalman filter and pattern recognition technology [44]. Data were recorded every  
 992  $\Delta t = 0.04$  s, and trajectories were then subjected to the same treatment.

### 993 Computational model

994 We use the same model to describe the time evolution of agents in the simulations and to  
 995 control the decisions of the robots in the experiments, albeit with different parameters to  
 996 accommodate for the different spatial and temporal scales in the two cases (see Table 3).

997 *Hemigrammus rhodostomus* displays a “burst-and-coast” swimming behavior char-  
 998 acterized by sequences of sudden speed increases called “kicks”, each followed by a  
 999 quasi-passive deceleration and gliding period along a near straight line until the next  
 1000 kick (Fig. 1C, S1 Video, S3 Video).

1001 In our model, we consider that a fish makes the decision to change its heading and  
 1002 to pick its new kick length and duration exactly at the onset of each kick [14]. The  
 1003 behavior of an agent  $i$  is thus described by a sequence of kicking times  $t_i^n$  at which  
 1004 the agent  $i$  performs its  $n$ -th kick. An agent selects a new heading depending on the  
 1005 *instantaneous* state of its environment (other fish; obstacles), as perceived exactly at  
 1006 the onset of a new kick, although the results of [28] suggest that the integration of  
 1007 the necessary information by an actual fish can take a few tenths of a second during  
 1008 the previous gliding period. Hence, at each of its kicking times  $t_i^n$ , the agent  $i$  collects  
 1009 the information of its instantaneous relative position and heading with respect to the  
 1010 obstacles and to the other agents, and selects the length and duration of its  $n$ -th kick,  $l_i^n$   
 1011 and  $\tau_i^n$  respectively, and its change of direction,  $\delta\phi_i^n$ . Each agent has its own sequence  
 1012 of kicking times, which are not necessarily equally spaced:  $t_i^{n+1} - t_i^n \neq t_i^n - t_i^{n-1}$ . In  
 1013 addition, the motion of the different agents is asynchronous and their respective kicking  
 1014 times are in general different. As the environment changes from one kick to another (the  
 1015 agent moves with respect to the obstacles, and the other agents move with respect to  
 1016 the agent), the quantities  $l_i^n$ ,  $\tau_i^n$ , and  $\delta\phi_i^n$  are updated at each kicking time of agent  $i$ ,  
 1017 according to the number and identity of the agents taken into account in the evaluation  
 1018 of the effect of social interactions. In the present work, the number of agents taken into  
 1019 account in the social interactions remains constant, while the identity of the neighbors  
 1020 considered to interact with an agent is updated at each kicking time of this focal agent.

1021 The behavior of agent  $i$  (fish or robot) is thus described by the following discrete-time  
 1022 decision model:

$$\vec{u}_i^{n+1} = \vec{u}_i^n + l_i^n \vec{e}(\phi_i^{n+1}), \quad (2)$$

$$\phi_i^{n+1} = \phi_i^n + \delta\phi_i^n, \quad (3)$$

1023 where  $\vec{u}_i^{n+1}$  and  $\phi_i^{n+1}$  are the vector position and the heading of agent  $i$  at the end of its  
 1024  $n$ -th kick, and  $\vec{e}(\phi_i^{n+1})$  is the unitary vector pointing in the direction of angle  $\phi_i^{n+1}$ . At  
 1025 the end of the  $n$ -th kick of agent  $i$ , the time is  $t_i^{n+1} = t_i^n + \tau_i^n$ , which is the next kicking  
 1026 time of agent  $i$ . Note that one or more agents can perform one or more kicks between  
 1027 two successive kicks of agent  $i$ . In that case, the kicking agent collects the information  
 1028 about agent  $i$  (relative position and heading) to perform its own kick, while agent  $i$  is  
 1029 simply in the gliding phase following its last kick.

1030 The kick length  $l_i^n$  is sampled at each kicking time of agent  $i$  from the bell-shaped  
 1031 distribution of kick lengths obtained in our experiments of fish swimming in pairs [14],  
 1032 whose mean value is  $l = 7$  cm. When the new computed position of the agent would be  
 1033 outside of the tank, a new kick length is sampled from the distribution. The typical  
 1034 speed of fish right after a kick was found to be  $v_0 \sim 14$  cm/s, and the speed was then  
 1035 found to decay exponentially during the gliding phase, with a relaxation time  $\tau_0 = 0.8$  s  
 1036 (a feature implemented in the model in [14]). Thus, the duration of the time step  $\tau_i^n$ ,  
 1037 updated at each kicking time of agent  $i$ , is determined by the length of the kick and the  
 1038 peak speed of the fish [14].

1039 The variation of the heading angle of agent  $i$  between two of its kicks is given by the  
 1040 sum of the variations induced by its environment, that is,

$$\delta\phi_i^n = \delta\phi_{w,i}^n + \delta\phi_{R,i}^n + \sum_{\langle j,i \rangle} \delta\phi_{i,j}^n, \quad (4)$$

1041 where  $\delta\phi_{w,i}^n$  is the angular variation caused by static obstacles (the wall of the fish tank  
 1042 or the border of the robot platform),  $\delta\phi_{R,i}^n$  is a random Gaussian white noise reflecting  
 1043 the spontaneous fluctuations in the motion of the agent, and  $\delta\phi_{i,j}^n$  is the angular variation  
 1044 induced by the social interaction of the agent  $i$  with the agent  $j$ .

1045 The notation  $\langle j, i \rangle$  indicates that the sum is performed over all the agents  $j$  considered  
 1046 to interact with agent  $i$ . The number  $k$  of agents considered to interact with an agent  
 1047 is part of what constitutes a social interaction strategy, and remains constant along  
 1048 the whole simulation. When  $k < N - 1$ , the identity of these agents depends on the  
 1049 strategy, but also on the instantaneous state of the system, so that their identity must  
 1050 be updated at each kicking time of the focal agent  $i$ . At each kicking time  $t_i^n$ , the agents  
 1051 are sorted according to the criterion used in the interaction strategy: the distance to the  
 1052 focal agent  $d_{ij}(t_i^n)$ , a random selection of neighbors, or the influence on the focal agent  
 1053  $\mathcal{I}_{ij}(t_i^n)$ . Once sorted, the  $k$  first agents are considered in the sum in Eq. (4).

1054 Each contribution to the angle variation can be expressed in terms of decoupled  
 1055 functions of the instantaneous state of the agents, that is, the distance and relative  
 1056 orientation to the wall  $r_w$  and  $\theta_w$ , and the distance  $d$ , viewing angle  $\psi$ , and relative  
 1057 alignment  $\phi$  between the focal fish and its considered neighbor (see Fig. 2A). The  
 1058 derivation of these functions is based on physical principles of symmetry of the angular  
 1059 functions and a sophisticated reconstruction procedure detailed in Calovi *et al.* [14] for  
 1060 the case of *H. rhodostomus* and in [15] for the general case of animal groups.

1061 For completeness, we show these functions in S9 Fig and present here their analytical  
 1062 expressions with the parameter values necessary to reproduce the simulations.

- 1063 • The repulsive effect of the wall is a centripetal force that depends only on the  
 1064 distance to the wall  $r_w$  and the relative angle of the heading to the wall  $\theta_w$ .

1065 Assuming that this dependence is decoupled, *i.e.*,  $\delta\phi_w(r_w, \theta_w) = F_w(r_w) O_w(\theta_w)$ ,  
 1066 we have:

$$F_w(r_w) = \gamma_w \exp \left[ - \left( \frac{r_w}{l_w} \right)^2 \right], \quad O_w(\theta_w) = \beta_w \sin(\theta_w) \left( 1 + 0.7 \cos(2\theta_w) \right), \quad (5)$$

1067 where  $\gamma_w = 0.15$  is the intensity of the force ( $F_w(0) = \gamma_w$ ),  $l_w = 0.06$  m is the range  
 1068 of the wall repulsion, and  $\beta_w = 1.9157$  is a normalization constant of the angular  
 1069 function  $O_w(\theta_w)$ , so that the mean of the squared function in  $[-\pi, \pi]$  is equal to 1,  
 1070 that is,  $(1/2\pi) \int_{-\pi}^{\pi} O_w^2(\theta) d\theta = 1$ . All angular functions are normalized in this way,  
 1071 in order to allow the direct comparison of their shape in the different interactions.

1072 These parameter values are those used in the model simulations. They also appear  
 1073 in Table 3, together with the values used in the experiments with robots.

- 1074 • The intensity of the stochastic spontaneous variation of heading  $\delta\phi_R$  depends on  
 1075 the distance to the wall  $r_w$ , and decreases as the fish gets closer to the wall and  
 1076 becomes constrained by the boundary of the tank:

$$\delta\phi_R(r_w) = \gamma_R \left( 1 - \alpha \exp \left[ - \left( \frac{r_w}{l_w} \right)^2 \right] \right) g, \quad (6)$$

1077 where  $\gamma_R = 0.45$ ,  $\alpha = 2/3$ , and  $g$  is a random number sampled from a standard  
 1078 normal distribution (zero mean; unit variance). Random variations are minimal at  
 1079 the border, where  $r_w = 0$ ,  $\delta\phi_R = \gamma_R(1 - \alpha)g$ , and become larger as the individual  
 1080 moves away from the border, *i.e.*, as  $r_w$  grows. Far from the border, the exponential  
 1081 goes to zero and  $\delta\phi_R = \gamma_R g$ .

- 1082 • The interaction between agents can be decomposed into two terms of attraction  
 1083 and alignment which depend only on the relative state of both interacting agents:

$$\delta\phi_{ij}(d_{ij}, \psi_{ij}, \phi_{ij}) = \delta\phi_{Att}^{ij} + \delta\phi_{Ali}^{ij}, \quad (7)$$

$$= \delta\phi_{Att}(d_{ij}, \psi_{ij}, \phi_{ij}) + \delta\phi_{Ali}(d_{ij}, \psi_{ij}, \phi_{ij}), \quad (8)$$

1084 where the relative state of fish  $j$  with respect to fish  $i$  is given by  $d_{ij}$ , the distance  
 1085 between them;  $\psi_{ij}$ , the viewing angle with which fish  $i$  perceives fish  $j$ ; and  
 1086  $\phi_{ij} = \phi_j - \phi_i$ , the difference between their heading angle.

1087 We then define the *influence*  $\mathcal{I}_{ij}(t)$  of a neighbor  $j$  on a focal individual  $i$  as the  
 1088 absolute contribution of this neighbor to the instantaneous heading change of the  
 1089 focal individual  $\delta\phi_i(t)$  in Eq. (4), that is, for  $j = 1, \dots, N$ ,  $j \neq i$ :

$$\mathcal{I}_{ij}(t) = |\delta\phi_{Att}^{ij}(t) + \delta\phi_{Ali}^{ij}(t)|. \quad (9)$$

1090 This precise definition is central to the implementation of the MOST INFLUENTIAL  
 1091 interaction strategy involving the  $k$  most influential neighbors of a given focal fish  $i$   
 1092 (*i.e.*, the  $k$  neighbors with the largest influence  $\mathcal{I}_{ij}(t)$ )

1093 Following [14], we assume that both the attraction and the alignment functions  
 1094  $\delta\phi_{Att}^{ij}$  and  $\delta\phi_{Ali}^{ij}$  can be decomposed as the product of three functions that each  
 1095 depend on only one of the three variables determining the relative state of the  
 1096 two fish. Thus, for the attraction interaction, we have  $\delta\phi_{Att}(d_{ij}, \psi_{ij}, \phi_{ij}) =$   
 1097  $F_{Att}(d_{ij}) O_{Att}(\psi_{ij}) E_{Att}(\phi_{ij})$ , where

$$F_{Att}(d) = \gamma_{Att} \left( \frac{d}{d_{Att}} - 1 \right) \frac{1}{1 + (d/l_{Att})^2}, \quad (10)$$

$$O_{Att}(\psi) = \beta_{Att} \sin(\psi) \left( 1 - 0.33 \cos(\psi) \right), \quad (11)$$

$$E_{Att}(\phi) = \lambda_{Att} \left( 1 - 0.48 \cos(\phi) - 0.31 \cos(2\phi) \right). \quad (12)$$

1098 Here,  $d_{Att} = 3$  cm is the distance at which the short-range repulsion of individual  
 1099 collision avoidance balances the long-range repulsion,  $\gamma_{Att} = 0.12$  is the intensity  
 1100 of the interaction, and  $l_{Att} = 20$  cm characterizes the range where attraction is  
 1101 maximum. The angular functions  $O_{Att}$  and  $E_{Att}$  are respectively normalized with  
 1102  $\beta_{Att} = 1.395$  and  $\lambda_{Att} = 0.9326$ . As already mentioned when describing the  
 1103 interaction with the wall, the three functional forms defined in (10–12) and the  
 1104 numerical values of the coefficients have been extracted from experimental data by  
 1105 means of a sophisticated procedure based on physical principles of symmetry of  
 1106 the angular functions [14,15]. The names of the angular functions stand precisely  
 1107 for their parity (Odd/Even).

1108 In the alignment, we have  $\delta\phi_{Ali}(d_{ij}, \psi_{ij}, \phi_{ij}) = F_{Ali}(d_{ij}) E_{Ali}(\psi_{ij}) O_{Ali}(\phi_{ij})$ , where

$$F_{Ali}(d) = \gamma_{Ali} \left( \frac{d}{d_{Ali}} + 1 \right) \exp \left[ - \left( \frac{d}{l_{Ali}} \right)^2 \right], \quad (13)$$

$$E_{Ali}(\psi) = \beta_{Ali} \left( 1 + 0.6 \cos(\psi) - 0.32 \cos(2\psi) \right), \quad (14)$$

$$O_{Ali}(\phi) = \lambda_{Ali} \sin(\phi) \left( 1 + 0.3 \cos(2\phi) \right), \quad (15)$$

1109 with  $d_{Ali} = 6$  cm,  $l_{Ali} = 20$  cm,  $\gamma_{Ali} = 0.09$ ,  $\beta_{Ali} = 0.9012$ ,  $\lambda_{Ali} = 1.6385$ .

1110 The parameter values are those derived in [14] for the simulation model when fish  
 1111 swim in pairs and are summarized in Table 3 (fish model and robots). More details  
 1112 regarding the model, including the extraction of the above interaction functions, can be  
 1113 found in [14].

1114 **Computational model in an unbounded domain.** Model simulations of agents  
 1115 swimming in an unbounded domain were carried out by removing the interaction with  
 1116 the wall (*i.e.*, by setting  $\gamma_w = 0$ ; the rest of parameter values being those given in  
 1117 Table 3).

1118 We have considered the MOST INFLUENTIAL and NEAREST interaction strategies, that  
 1119 is, paying respectively attention to the  $k$  most influential neighbors or to the  $k$ -nearest  
 1120 neighbors, for  $k = 1, 2, 3$ , and 4, and the case where agents do not interact with each  
 1121 other ( $k = 0$ ). Group cohesion and polarization are averaged over a large number of  
 1122 simulation runs  $n$ :  $\langle C(t) \rangle = (1/n) \sum_{i=1}^n C_i(t)$ , where  $C_i(t)$  is the group cohesion at time  $t$   
 1123 in the  $i$ -th run. We used  $n = 1000$ . The duration of each simulation was sufficiently  
 1124 long to produce a total number of  $10^4$  kicks per run among the 5 agents ( $\sim 2.7$  hours).  
 1125 A second series of simulations was carried out to produce  $5 \times 10^4$  kicks ( $\sim 13.5$  hours),  
 1126 finding the same qualitative results. Initial conditions of each run were always different,  
 1127 with all agents located at less than  $R = 25$  cm (the radius of the arena) from the origin  
 1128 of coordinates.

1129 We first analyzed the impact on group cohesion and polarization (Fig. 9 and Fig. 10)  
 1130 of reducing the attraction range in groups of  $N = 5$  agents by truncating the attraction  
 1131 intensity function  $F_{Att}$  when the neighbor is at a distance  $d_{ij} > d_{cut}$  from the focal agent:  
 1132  $F_{Att}(d_{ij}) = 0$ , if  $d_{ij} > d_{cut}$ . For each value of  $d_{cut}$ , the mean cohesion was calculated as  
 1133 the average over the last 10% of kicks over the 1000 runs carried out to obtain  $\langle C(t) \rangle$ , and  
 1134 this, for both considered strategies and each value of  $k$ . When  $d_{cut}$  is sufficiently large,  
 1135 the attraction range is sufficiently long and  $\langle C(t) \rangle$  is close to the value corresponding to  
 1136 the mean cohesion of the group when  $F_{Att}$  is not truncated. When  $d_{cut}$  is smaller than  
 1137 a critical cut-off  $d_{cut}^*$ , the attraction range is too short and the agents simply diffuse,  
 1138 with  $\langle C(t) \rangle \sim t$  growing linearly in time Fig. 9.

1139 We then analyzed the group cohesion and polarization (Fig. 10 and S7 Fig) *i*) in  
 1140 large groups of  $N = 6, \dots, 70$  agents for the MOST INFLUENTIAL strategy with  $k = 1$ , *ii*)

1141 in a group of size  $N = 20$ , for different values of the number of nearest neighbors  $k$  with  
 1142 which agents interact, and *iii*) in groups of size  $N = 5, \dots, 26$ , where agents interact with  
 1143 their  $k$  nearest neighbors, for all the values of  $k$  between 1 and  $N - 1$ , except for  $N = 22$ ,  
 1144 24 and 26, where we limited the simulations to the interval of interest  $k = 8, \dots, 12$ . For  
 1145 each combination of group size  $N$  and number of neighbors  $k$  considered, the number of  
 1146 simulations, their duration, and the averaging procedure were the same as the ones used  
 1147 in the analysis of the groups of size  $N = 5$ .

## 1148 Quantification of the collective behavior

1149 We characterize the collective behavioral patterns by means of five observables quantifying  
 1150 the behavior of the group in the tank and the behavior of individuals inside the group. We  
 1151 first write the coordinates of the position  $\vec{u}_B = (x_B, y_B)$  and the velocity  $\vec{v}_B = (v_x^B, v_y^B)$   
 1152 of the barycenter  $B$  (center of mass) of the group with respect to the reference system  
 1153 of the tank:

$$x_B(t) = \frac{1}{N} \sum_{i=1}^N x_i(t), \quad v_x^B(t) = \frac{1}{N} \sum_{i=1}^N v_x^i(t), \quad (16)$$

1154 with similar expressions for  $y_B(t)$  and  $v_y^B(t)$ . The heading angle of the barycenter is  
 1155 then given by  $\phi_B = \text{ATAN2}(v_y^B, v_x^B)$ .

1156 The barycenter defines a system of reference in which the relative position and velocity  
 1157 of a fish, that we denote with a bar, are such that  $\bar{x}_i = x_i - x_B$  and  $\bar{v}_x^i = v_x^i - v_x^B$   
 1158 (same expressions for the  $y$ -components). In the reference system of the barycenter, the  
 1159 angle of the position of a fish is given by  $\bar{\theta}_i = \text{ATAN2}(\bar{y}_i, \bar{x}_i)$ , so the relative heading in  
 1160 this reference system is  $\bar{\phi}_i = \text{ATAN2}(\bar{v}_y^i, \bar{v}_x^i) \neq \phi_i - \phi_B$ . We can thus define the angle of  
 1161 incidence of a fish with respect to a circle centered at the barycenter as  $\bar{\theta}_w^i = \bar{\phi}_i - \bar{\theta}_i$ .  
 1162 The angle  $\bar{\theta}_w^i$  is the equivalent to the angle of incidence to the wall  $\theta_w^i$  that we use in  
 1163 the reference system of the tank, and serves to measure the angular velocity of a fish  
 1164 with respect to the barycenter, in the reference system of the barycenter.

1165 The five observables used to quantify the behavior of a group are defined as follows:

- 1166 1. Group cohesion  $C(t) \in [0, R]$ :

$$C(t) = \sqrt{\frac{1}{N} \sum_{i=1}^N \|\vec{u}_i - \vec{u}_B\|^2}, \quad (17)$$

1167 where  $\|\vec{u}_i - \vec{u}_B\|$  is the distance from fish  $i$  to the barycenter  $B$  of the  $N$  fish.

1168 Low values of  $C(t)$  correspond to highly cohesive groups, while high values of  $C(t)$   
 1169 (in particular, comparable to the radius of the tank) imply that individuals are  
 1170 spatially dispersed.

- 1171 2. Group polarization  $P(t) \in [0, 1]$ :

$$P(t) = \frac{1}{N} \left\| \sum_{i=1}^N \vec{e}_i(t) \right\|, \quad (18)$$

1172 where  $\vec{e}_i = \vec{v}_i / \|\vec{v}_i\| = (\cos(\phi_i), \sin(\phi_i))$  is the unit vector in the direction of motion  
 1173 of the individual fish, given by its velocity vector  $\vec{v}_i$ .

1174 A value of  $P$  close to 1 would mean that the  $N$  individual headings are aligned  
 1175 and point in the same direction, while a value of  $P$  close to 0 would mean that the  
 1176  $N$  vectors point in different directions, but can also mean that vectors are collinear

1177 and with opposite direction (*e.g.*, for  $N$  even, half of the vectors point North, the  
 1178 other half point South) so that they cancel each other. Similarly, when  $N = 5$  and  
 1179 two normalized velocity vectors cancel each other (*e.g.*, when 4 fish swim in the  
 1180 same direction  $\vec{e}$  and one fish swims in the opposite direction  $-\vec{e}$ ) would give rise  
 1181 to a resultant vector of norm  $P = (4 \times 1 - 1)/5 = 3/5 = 0.6$ , and if two pairs of  
 1182 fish cancel each other, then  $P = (3 \times 1 - 2 \times (-1))/5 = 1/5 = 0.2$ .

1183 Note that uncorrelated headings would lead to  $P \sim 1/\sqrt{N}$ , which becomes small  
 1184 only for large group size  $N$ , but which is markedly lower than 1 for any  $N \geq 5$ .

1185 3. Distance of the barycenter to the wall  $r_w^B(t) \in [0, R]$ :

$$r_w^B(t) = R - \sqrt{(x_B(t))^2 + (y_B(t))^2}, \quad (19)$$

1186 Note that when the individuals move in a cohesive group,  $r_w^B$  is typically of the  
 1187 same order as the mean distance of agents to the wall  $\langle r_w \rangle = (1/N) \sum_{i=1}^N r_w^i$ .  
 1188 When the group is not cohesive,  $r_w^B$  is of order of the radius of the tank.

1189 4. Relative angle of the barycenter heading to the wall  $\theta_w^B(t) \in [-\pi, \pi]$ :

$$\theta_w^B(t) = \text{ATAN2}(v_y^B(t), v_x^B(t)). \quad (20)$$

1190 When the group swims along the wall  $\theta_w^B(t) \approx \pm\pi/2$  (*i.e.*,  $\theta_w^B(t) \approx \pm 90^\circ$ ).

1191 5. Index of collective counter-milling and super-milling  $Q(t) \in [-1, 1]$ :

$$Q(t) = \left( \frac{1}{N} \sum_{i=1}^N \sin(\theta_w^i(t)) \right) \times \text{SIGN} \left( \frac{1}{N} \sum_{i=1}^N \sin(\theta_w^i(t)) \right) \quad (21)$$

$$= \Gamma_B(t) \times \text{SIGN}(\Gamma(t)). \quad (22)$$

1192 A group of fish rotating around the center of the tank with a rotation index  $\Gamma(t)$   
 1193 (defined in Eq. (22); similar to an angular momentum) would display a counter-  
 1194 milling behavior if the individual fish also rotate around the barycenter of the group  
 1195 and both directions of rotation are opposite. The first sum between parentheses  
 1196 in Eq. (21) is the index of rotation of the fish with respect to the barycenter of  
 1197 the group, denoted by  $\Gamma_B(t)$  in Eq. (22). Multiplying by the sign of  $\Gamma(t)$  means  
 1198 that when  $Q(t) < 0$ , both directions are opposite and the fish exhibit a *collective*  
 1199 *counter-milling behavior*, while when  $Q(t) > 0$ , both rotations are in the same  
 1200 direction and the fish exhibit a *collective super-milling behavior*.

1201 Thus, a group of 5 individuals turning around the center of the tank in a rigid  
 1202 formation that always points North, like the fingertips of the hand when cleaning  
 1203 a window, would correspond to a perfect counter-milling behavior. On the other  
 1204 hand, a situation where individuals rotate around the center of the tank as if they  
 1205 were fixed to a vinyl record, so that trajectories are perfect circles and individuals  
 1206 far from the center of the tank move faster than those close to the center, would  
 1207 correspond to a zero-milling state. Actual groups of fish present an intermediate  
 1208 behavior between these two situations, with a clear bias towards negative values of  
 1209  $Q(t)$  (see Fig. 3 for fish, S4 Video for robots, and Fig. 8 for fish, model fish, and  
 1210 robots).

1211 Collective behavior is thus quantified by means of the probability density functions  
 1212 of these quantities. In addition, density maps are presented in order to illustrate the  
 1213 correlations between the polarization  $P$  and the group cohesion  $C$  in fish experiments,

1214 model simulations, and robot experiments (S1 Fig–S4 Fig). We consider two normaliza-  
 1215 tions: *i*) with the total number of data, to highlight the significant regions of the map  
 1216 and neglect the regions where the data are scarce (S1 Fig for the fish model, and S3  
 1217 Fig for robot experiments); *ii*) with the total number of data in a given range of the  
 1218 polarization, so that each row in the map is a PDF of  $C$  for a given  $P$  (S2 Fig for the  
 1219 fish model, and S4 Fig for robot experiments). Spatial distances in the model and robot  
 1220 experiments are rescaled with the respective scaling factor  $\lambda_M = 0.87$  and  $\lambda_R = 0.35$  to  
 1221 allow for a direct comparison of our two spatial quantifiers ( $C$  and  $r_w^B$ ) with the results  
 1222 of fish experiments (the three other quantifiers  $P$ ,  $\theta_w^B$ , and  $Q$  are not affected by this  
 1223 rescaling).

## 1224 Quantifier for the similarity of probability distribution functions

1225 In the Results section, we qualitatively compare the probability distribution functions  
 1226 (PDF) of the group cohesion, polarization, distance to the wall, angle with respect to  
 1227 the wall, and counter-milling index featured in Figs. 4–8, for the 3 interaction strategies  
 1228 (NEAREST; RANDOM; MOST INFLUENTIAL), and for  $k = 1, 2, 3$  interacting neighbors (as  
 1229 well as the cases  $k = 0$  – no interaction – and  $k = 4$ ).

1230 Here, we consider the Hellinger distance  $D(F|G)$  [45,46] to precisely quantify the  
 1231 “similarity” of two PDF  $F(x)$  and  $G(x)$  for the same observable  $x$  (one of the 5 listed  
 1232 above that we have considered):

$$D(F|G) = \frac{1}{2} \int \left( \sqrt{F(x)} - \sqrt{G(x)} \right)^2 dx = 1 - \int \sqrt{F(x)} \sqrt{G(x)} dx, \quad (23)$$

1233 where we have used the normalization of the PDF,  $\int F(x) dx = \int G(x) dx = 1$ , to  
 1234 obtain the last equality. The first definition of  $D(F|G)$  makes clear that it measures the  
 1235 overall difference between  $F(x)$  and  $G(x)$ , while the second equivalent definition has a  
 1236 nice interpretation in terms of the *overlap* of both PDF. Indeed, the second definition  
 1237 measures the distance from unity of the scalar product of  $\sqrt{F(x)}$  and  $\sqrt{G(x)}$  seen as  
 1238 vectors of unit Euclidean norm (a consequence of the normalization,  $\int \sqrt{F(x)}^2 dx = 1$ ).

1239 The Hellinger distance is zero if and only if  $F(x) = G(x)$ , and it always satisfies  
 1240  $D(F|G) \leq 1$ . The upper bound  $D(F|G) = 1$  is reached whenever the supports of the  
 1241 two PDF are not intersecting, so that  $F(x) \times G(x) = 0$ , for all values of  $x$ . In practice,  
 1242 a value of  $D(F|G) \geq 0.1$  points to the two PDF being markedly dissimilar.

1243 Of course, using the Hellinger distance is an arbitrary choice and other distances  
 1244 (like the Kolmogorov-Smirnov distance) could lead to slightly different relative dis-  
 1245 tances/errors, but would not change our conclusions when the PDF are markedly  
 1246 different. In particular, the fact that the MOST INFLUENTIAL strategy is the strategy for  
 1247  $k = 1$  leading to the best agreement with fish experiments would be recovered by any  
 1248 meaningful quantifier.

1249 We have computed the Hellinger distance between PDF measured in fish experiments  
 1250 and the corresponding PDF measured in the fish model simulations (Table 1) and  
 1251 in robots experiments (Table 2), hence providing a more precise, albeit not unique,  
 1252 quantification of their similarity.

## 1253 Acknowledgments

1254 We thank the three anonymous referees for their thoughtful comments on the manuscript.  
 1255 We are grateful to Patrick Arrufat and Gérard Latil for technical assistance.

1256 **References**

- 1257 1. D. J. T. Sumpter (2010) *Collective Animal Behavior*. Princeton, NJ: Princeton  
1258 University Press.
- 1259 2. I. D. Couzin (2002) Collective cognition in animal groups. *Trends in Cognitive  
1260 Science*, 13(1):36433.
- 1261 3. M. Moussaïd, S. Garnier, G. Theraulaz and D. Helbing (2009) Collective infor-  
1262 mation processing in swarms, flocks and crowds. *Topics in Cognitive Science* 1,  
1263 469–497.
- 1264 4. S. Camazine, J. L. Deneubourg, N. Franks, J. Sneyd, G. Theraulaz and  
1265 E. Bonabeau (2001) *Self-Organization in Biological Systems*. Princeton, NJ: Prince-  
1266 ton University Press.
- 1267 5. I. D. Couzin and J. Krause (2003) Self-organization and collective behavior in  
1268 vertebrates. *Advances in the Study of Behavior* 32: 1–75.
- 1269 6. U. Lopez, J. Gautrais, I. D. Couzin and G. Theraulaz (2012) From behavioural  
1270 analyses to models of collective motion in fish schools. *Interface Focus* 2:693–707.
- 1271 7. A. Cavagna, A. Cimarelli, I. Giardina, G. Parisi, R. Santagati, F. Stefanini and  
1272 R. Tavarone (2010) From empirical data to inter-individual interactions: unveiling  
1273 the rules of collective animal behavior. *Mathematical Models and Methods in  
1274 Applied Sciences* 20:1491–1510.
- 1275 8. D. J. T. Sumpter (2006) The principles of collective animal behaviour. *Philoso-  
1276 phical Transactions of the Royal Society B: Biological Sciences* 361 (1465):5–22.
- 1277 9. T. Sasaki and S. C. Pratt (2018) The Psychology of Superorganisms: Collective  
1278 Decision Making by Insect Societies. *Annual Review of Entomology* 63:259–275.
- 1279 10. C. Detrain and J. L. Deneubourg (2006) Self-organized structures in a superorgan-  
1280 ism: Do ants “behave” like molecules? *Physics of Life Reviews* 3(3):162–187.
- 1281 11. C. Detrain and J. L. Deneubourg (2008) Collective decision-making and foraging  
1282 patterns in ants and honeybees. *Advances in Insect Physiology* 35:123–173.
- 1283 12. T. D. Seeley (1996) *Wisdom of the Hive*. Cambridge, MA: Harvard Univ. Press.
- 1284 13. T. D. Seeley (2010) *Honeybee Democracy*. Princeton, NJ: Princeton Univ. Press.
- 1285 14. D. S. Calovi, A. Litchinko, V. Lecheval, U. Lopez, A. Pérez Escudero, H. Chaté,  
1286 C. Sire, G. Theraulaz (2018) Disentangling and modeling interactions in fish with  
1287 burst-and-coast swimming reveal distinct alignment and attraction behaviors.  
1288 *PLoS Comput. Biol.* 14(1):e1005933.
- 1289 15. R. Escobedo, V. Lecheval, V. Papaspyros, F. Bonnet, F. Mondada, C. Sire, and  
1290 G. Theraulaz (2019). A data-driven method for reconstructing and modelling  
1291 social interactions in animal groups. <https://doi.org/10.1101/816777>.
- 1292 16. J. K. Parrish, S. V. Viscido and D. Grunbaum (2002) Self-organized fish schools:  
1293 An examination of emergent properties. *Biological Bulletin* 202:296–305.
- 1294 17. T. Vicsek and A. Zafeiris (2012) Collective motion. *Physics Reports* 517: 71–14.
- 1295 18. I. Aoki (1982) A simulation study on the schooling mechanism in fish. *Bull. J.  
1296 Soc. Sci. Fish* 48(8):1081–1088.

- 1297 19. I. D. Couzin, J. Krause, R. James, G. Ruxton and N. Franks (2002) Collective  
1298 memory and spatial sorting in animal groups. J. Theor. Biol. 218(5):1–11.
- 1299 20. T. Vicsek, A. Cziřok, E. Ben-Jacob, I. Cohen and O. Shochet (1995) Novel type  
1300 of phase transition in a system of self-driven particles. Physical Review Letters  
1301 75: 226–1229.
- 1302 21. M. Ballerini et al.(2008) Interaction ruling animal collective behavior depends on  
1303 topological rather than metric distance: Evidence from a Field Study. Proc. Natl.  
1304 Acad. Sci. USA 105:1232–1237.
- 1305 22. M. Camperi, A. Cavagna, I. Giardina, G. Parisi and E. Silvestri (2012) Spa-  
1306 tially balanced topological interaction grants optimal cohesion in flocking models.  
1307 Interface Focus 2:715–725.
- 1308 23. J. Gautrais *et al.* (2012) Deciphering interactions in moving animal groups. PLoS  
1309 Comp. Biol. 8(9):e1002678.
- 1310 24. S. B. Rosenthal, C. R. Twomey, A. T. Hartnett, H. S. Wu, and I. D. Couzin (2015)  
1311 Revealing the hidden networks of interaction in mobile animal groups allows  
1312 prediction of complex behavioral contagion. Proc. Natl. Acad. Sci. USA 112  
1313 15):4690–4695.
- 1314 25. B. H. Lemasson, J.. J. Anderson and R.A. Goodwin (2009) Collective motion  
1315 in animal groups from a neurobiological perspective: the adaptive benefits of  
1316 dynamic sensory loads and selective attention. Journal of Theoretical Biology  
1317 261(4):501–510.
- 1318 26. B.. H. Lemasson, J.. J. Anderson and R.A. Goodwin (2013) Motion-guided atten-  
1319 tion promotes adaptive communication during social navigation. Proceedings of  
1320 the Royal Society of London B: Biological Sciences 280(1754):20122003.
- 1321 27. A. M. Calvao and E. Brigatti (2014) The role of neighbours selection on cohesion  
1322 and order of swarms. PLoS ONE 9(5): e94221.
- 1323 28. L. Jiang, L. Giuggioli, A. Perna, R. Escobedo, V. Lecheval, C. Sire, Z. Han, and  
1324 G. Theraulaz (2017) Identifying influential neighbors in animal flocking. PLoS  
1325 Comput. Biol. 13:e1005822.
- 1326 29. Y. Katz, K. Tunstrøm, C. Ioannou, C. Huepe, and I. D. Couzin (2011) Inferring  
1327 the structure and dynamics of interactions in schooling fish. Proc. Natl. Acad.  
1328 Sci. USA 108(46):18720–18725.
- 1329 30. A. E. Turgut, H. Çelikkanat, F. Gökçe, and E. Şahin (2008) Self-organized flocking  
1330 in mobile robot swarms. Swarm Intelligence 2:97–120.
- 1331 31. C. Muro, R. Escobedo, L. Spector, and R. P. Coppinger (2011) Wolf-pack (*Canis*  
1332 *lupus*) hunting strategies emerge from simple rules in computational simulations.  
1333 Behav. Processes 88(3):192–197.
- 1334 32. D. S. Calovi, U. Lopez, S. Ngo, C. Sire, H. Chaté, and G. Theraulaz (2014)  
1335 Swarming, Schooling, Milling: Phase diagram of a data-driven fish school model.  
1336 New J. Phys., 16:015026.
- 1337 33. R. Dukas (2002) Behavioural and ecological consequences of limited attention.  
1338 Phil. Trans. R. Soc. Lond. B 357:1539–1547.

- 1339 34. Nagy M., Akos Z., Biro D., and Vicsek T. (2010) Hierarchical group dynamics in  
1340 pigeon flocks. Nature 464:890–893.
- 1341 35. Herbert-Read J. E., Perna A., Mann R. P., Schaerf, T. M., Sumpter D. J., and  
1342 Ward A. J. (2011) Inferring the rules of interaction of shoaling fish. Proc. Natl.  
1343 Acad. Sci. USA 108(46):18726–18731.
- 1344 36. V. Lecheval, L. Jiang., P. Tichit, C. Sire, C. K. Hemelrijk, and G. Theraulaz (2018)  
1345 Social conformity and propagation of information in collective U-turns of fish  
1346 schools. Proc. Roy. Soc. B, 285:20180251.
- 1347 37. A. Huth and C. Wissel (1992). The simulation of the movement of fish schools. J.  
1348 Theor. Biol. 156(3):365–385.
- 1349 38. H. S. Niwa (1994). Self-organizing dynamic model of fish schooling. J. Theor. Biol.  
1350 171(2):123–136.
- 1351 39. N. W. Bode, D. W. Franks, and A. J. Wood (2010). Limited interactions in flocks:  
1352 relating model simulations to empirical data. J. R. Soc. Interface 8:301–304.
- 1353 40. E. I. Knudsen (2018) Neural Circuits That Mediate Selective Attention: A Com-  
1354 parative Perspective. Trends in Neurosciences, 41:789–805.
- 1355 41. C. Reynolds (1987) Flocks, herds and schools: A distributed behavioral model.  
1356 Computer Graphics 21(4) (SIGGRAPH '87 Conference Proceedings), pp. 25–34.
- 1357 42. X. Hu (2005) Applying robot-in-the-loop-simulation to mobile robot systems. In  
1358 Advanced Robotics, 2005. ICAR'05 Proceedings, 12th International Conference  
1359 on, p. 506–513.
- 1360 43. A. Pérez-Escudero, J. Vicente-Page, R. C. Hinz, S. Arganda, and G. G. de Polavieja  
1361 (2014) idTracker: tracking individuals in a group by automatic identification of  
1362 unmarked animals. Nature Methods 11:743–748.
- 1363 44. J. Goncalves, J. Lima, and P. Costa (2008) Real-time localization of an omni-  
1364 directional mobile robot resorting to odometry and global vision data fusion:  
1365 An EKF approach. IEEE International Symposium on Industrial Electronics, pp.  
1366 1275–1280.
- 1367 45. A. Basu, I. R. Harris, S. Basu (1997). Minimum distance estimation: the approach  
1368 using density based distances. In: G. S. Maddala, C. R. Rao (Eds.), Handbook of  
1369 Statistics, Vol. 15, Robust Inference. Elsevier Science, New York, NY, pp. 21–48.
- 1370 46. R. Beran (1977). Minimum Hellinger distance estimates for parametric models.  
1371 Annals of Statistics 5:445–463.

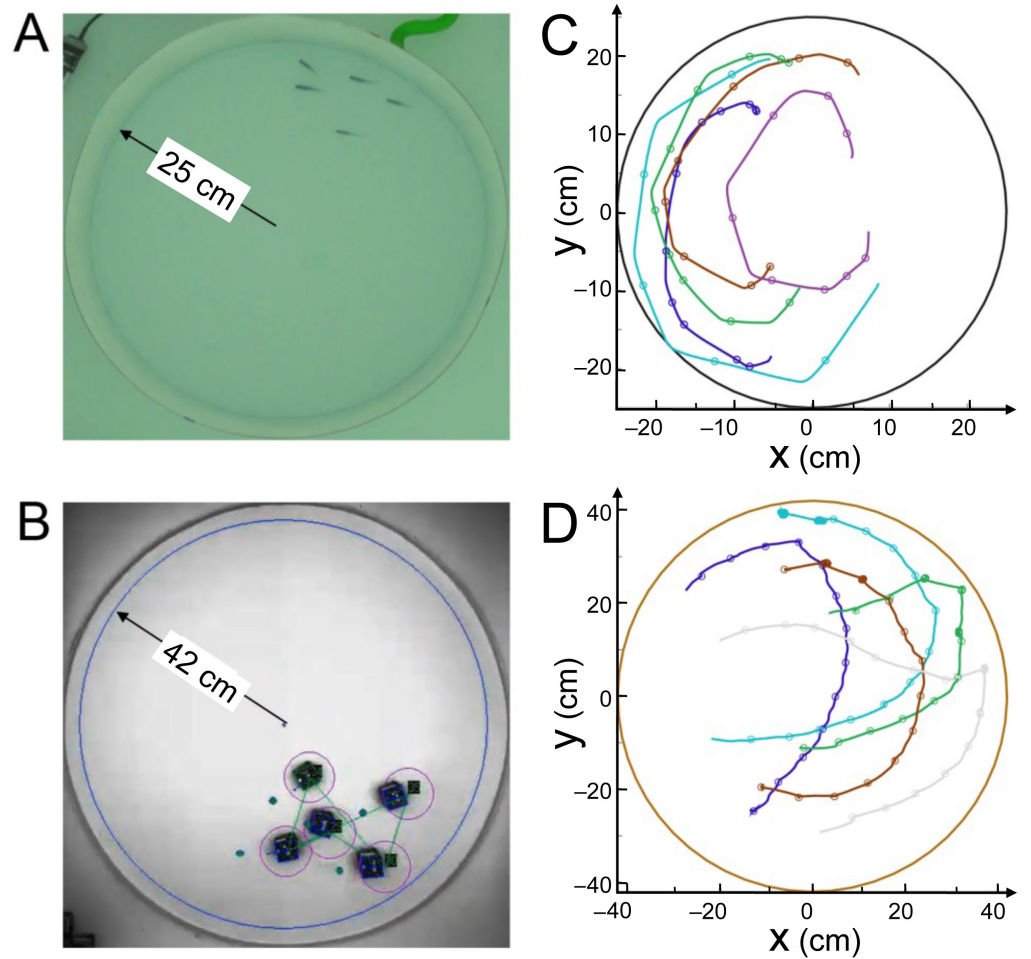


**Fig 1. Experimental setups and tracking.** (A) Experiments with 5 fish swimming in a tank of radius  $R_{\text{fish}} = 25$  cm. (B) 5 robots running in a platform of radius  $R_{\text{robot}} = 42$  cm. (C) Individual fish trajectories over 4 seconds. The circles represent the onset of bursts, when speed is minimum. (D) Individual trajectories in one robotic experiment over 24 seconds. The circles indicate the decisions of the robots to select a new target place, when individual speed is minimum.

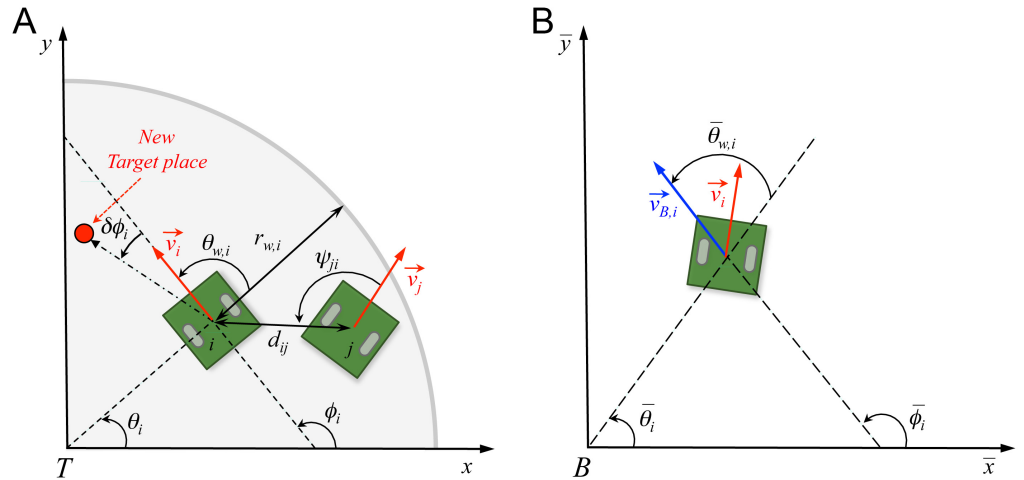


**Fig 2. Angles and reference systems.** (A) Distances, angles, and velocity vectors of agents  $i$  and  $j$  in the absolute reference system centered in  $T(0, 0)$ . Positive values of angles are fixed in the anticlockwise direction.  $\theta_i$  is the position angle of agent  $i$  with respect to  $T$  and the horizontal line;  $r_{w,i}$  is the distance of agent  $i$  from the nearest wall;  $\phi_i$  is the heading angle of agent  $i$ , determined by its velocity vector  $\vec{v}_i$ ;  $\theta_{w,i}$  is the relative angle of agent  $i$  with the wall;  $d_{ij}$  is the distance between agents  $i$  and  $j$ ;  $\psi_{ij}$  is the viewing angle with which agent  $i$  perceives agent  $j$ , *i.e.*, the angle between the velocity of  $i$  and the vector  $\vec{i}j$  (we show the angle  $\psi_{ji} \neq \psi_{ij}$  with which  $j$  perceives  $i$ , for the sake of readability of the figure);  $\phi_{ij} = \phi_j - \phi_i$  is the difference of heading between agents  $i$  and  $j$ , and  $\delta\phi_i$  is the variation of heading of agent  $i$ . (B) Relative reference system centered in the barycenter of the group  $B(x_B, y_B)$ . Relative variables are denoted with a bar. Angle  $\bar{\theta}_{w,i} = \bar{\phi}_i - \bar{\theta}_i$  is the angle of incidence of the relative speed of agent  $i$  with respect to a circle centered in  $B$ .

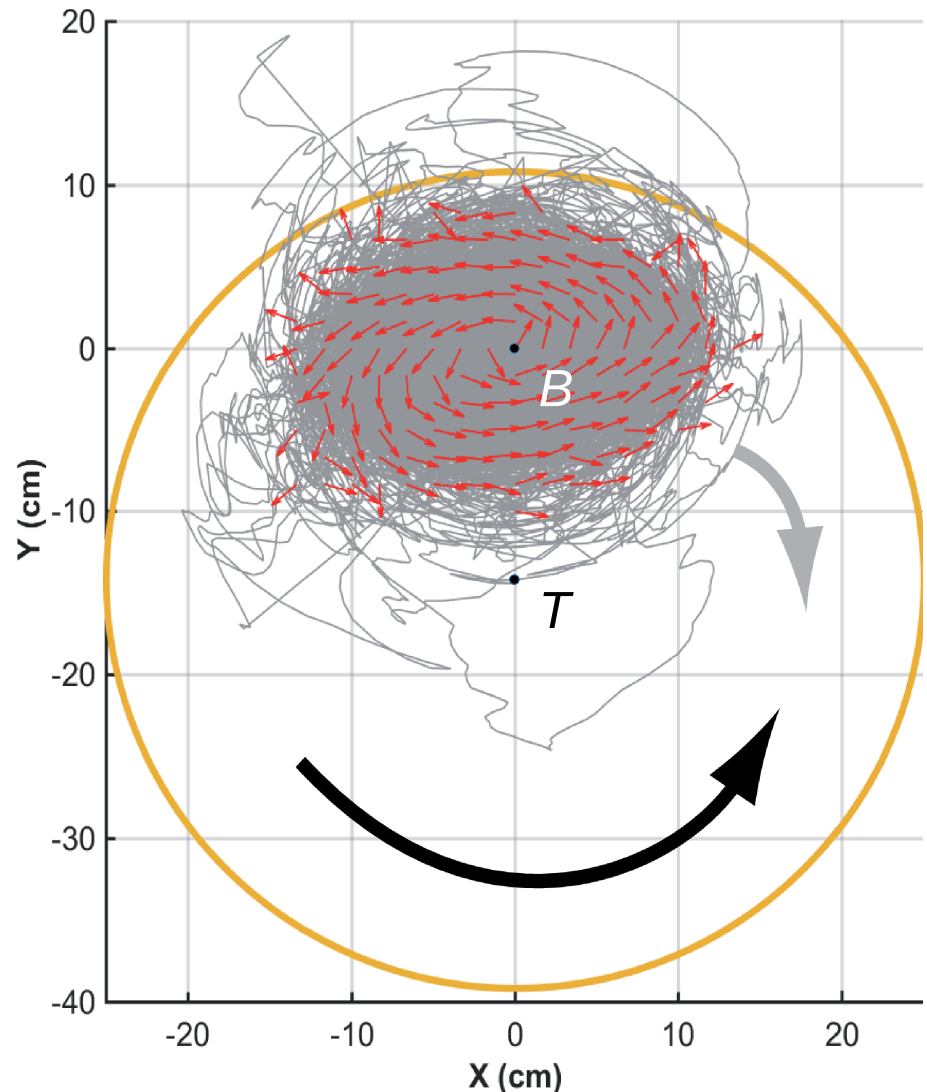


**Fig 3. Counter-milling in fish experiments.** Individual fish (small red arrows) turn counter-clockwise (CCW) around their barycenter, here located at  $B(0,0)$ , while the fish group rotates clockwise (CW) around the center of the tank, located at  $T(0,-14)$  in the reference system of the barycenter. Red arrows (of same length) denote relative fish heading, gray lines denote relative trajectories, and large orange circle denotes the average relative position of the border of the tank. The wide black arrow shows the direction of rotation of individual fish with respect to  $B$  (CCW), opposite to the wide gray arrow showing the direction of rotation of the group with respect to  $T$  (CW).

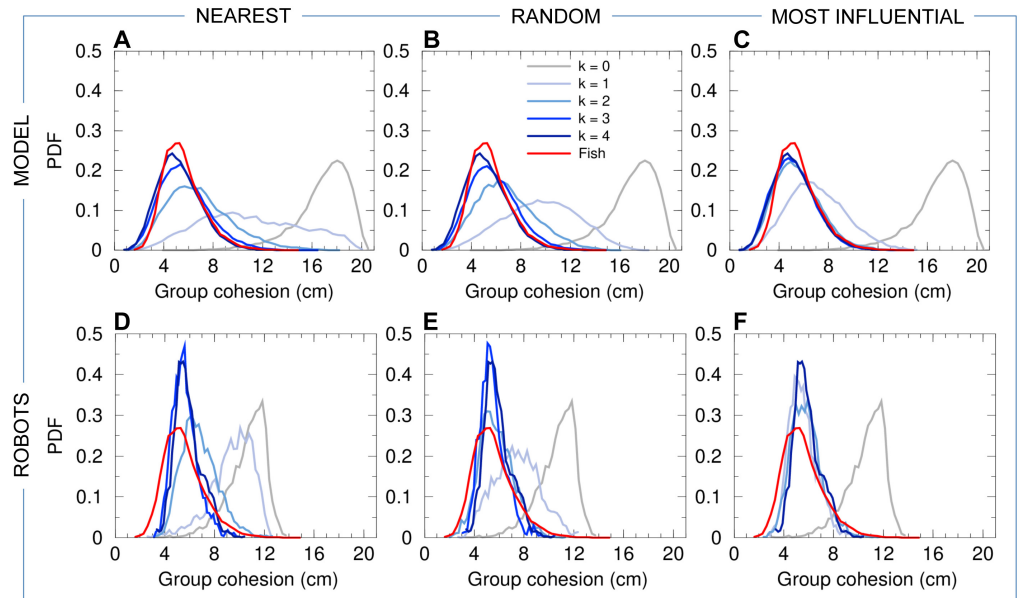


**Fig 4. Group cohesion.** Probability density functions (PDF) of the group cohesion  $C$  for the experiments with 5 fish (red line in all panels), model simulations (panels ABC), and experiments with 5 robots (panels DEF), compared to the corresponding null models ( $k = 0$ , no interaction between individuals) in both simulations and robots (gray line in all panels). Distances have been rescaled by  $\lambda_M = 0.87$  for the model simulations, and by  $\lambda_R = 0.35$  for the robot experiments. The intensity of blue is proportional to the number of neighbors interacting with a focal individual (agent or robot), from  $k = 1$  (light blue) to  $k = 4$  (dark blue). Interaction strategies involve the  $k$  NEAREST neighbors (panels AD),  $k$  RANDOM neighbors (panels BE), and the  $k$  MOST INFLUENTIAL neighbors (panels CF).

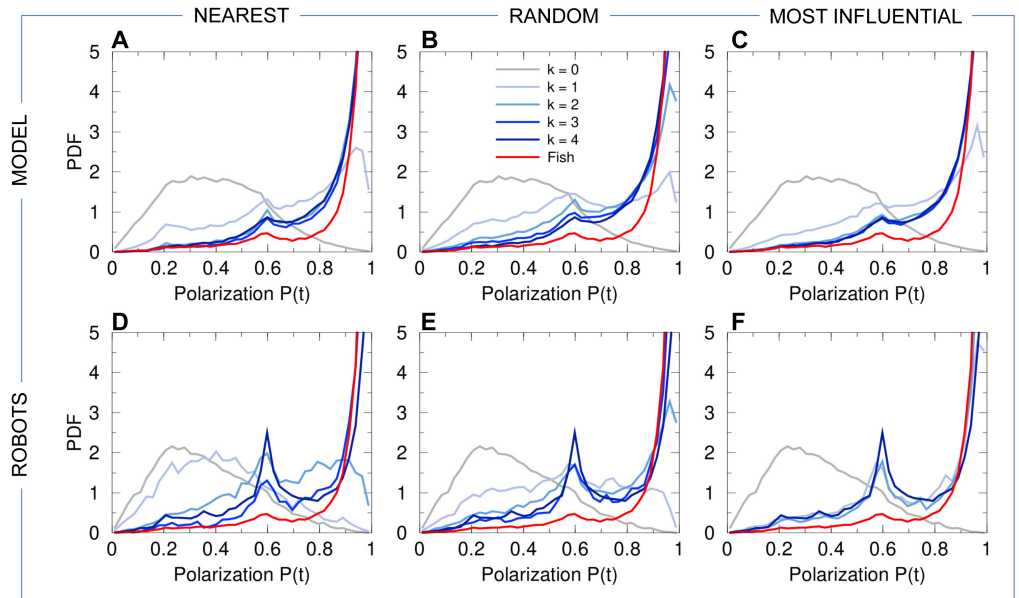


**Fig 5. Group polarization.** PDF of the group polarization  $P$  for fish experiments (red line in all panels), model simulations (panels ABC), and robot experiments (panels DEF), compared to the corresponding null models ( $k = 0$ , no interaction between individuals) in both simulations and robots (gray line in all panels). Curves for agents (fish model and robots) are in blue and gray, depending on the value of  $k$  (see legend in panel B). Interaction strategies involve the  $k$  NEAREST neighbors (panels AD),  $k$  RANDOM neighbors (panels BE), and the  $k$  MOST INFLUENTIAL neighbors (panels CF).

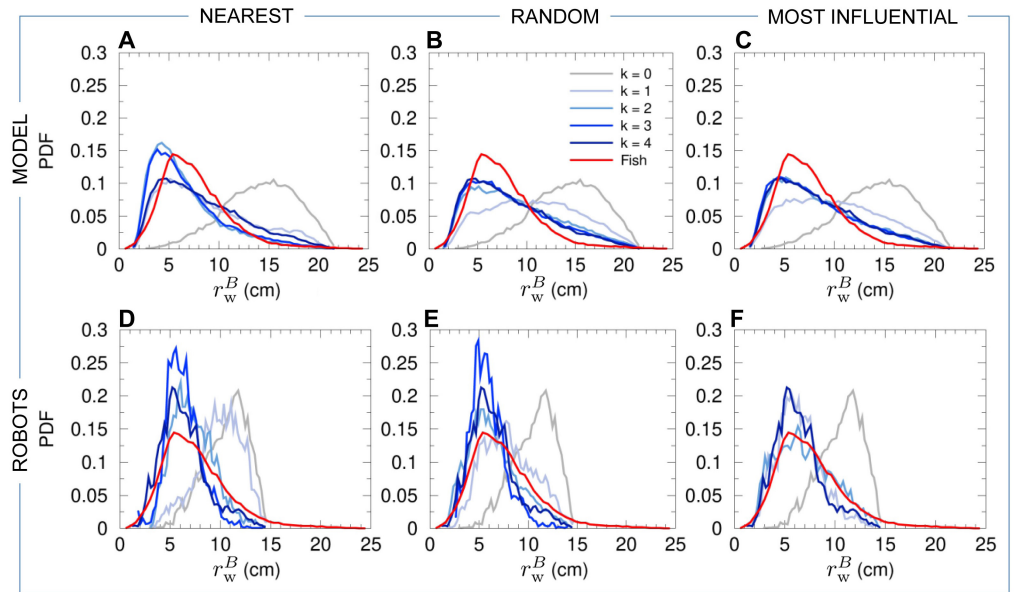


**Fig 6. Distance of the barycenter of the individuals to the wall.** PDF of the distance  $r_w^B$  of the barycenter of the individuals from the wall for fish experiments (red line in all panels), model simulations (panels ABC), and robot experiments (panels DEF), compared to the corresponding null models ( $k = 0$ , no interaction between individuals) in both simulations and robots (gray line in all panels). Distances have been rescaled by  $\lambda_M = 0.87$  for the model simulations, and by  $\lambda_R = 0.35$  for the robot experiments. Curves for agents (fish model and robots) are in blue and gray, depending on the value of  $k$  (see legend in panel B). Interaction strategies involve the  $k$  NEAREST neighbors (panels AD),  $k$  RANDOM neighbors (panels BE), and the  $k$  MOST INFLUENTIAL neighbors (panels CF).

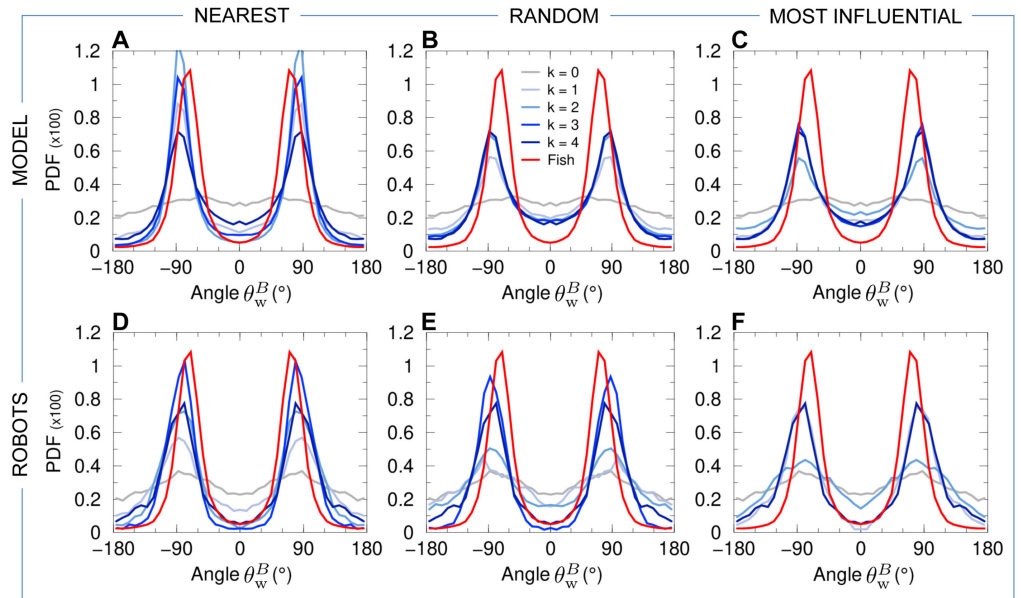


**Fig 7. Relative angle of the heading of the barycenter of the group with the wall.** PDF of the relative angle  $\theta_w^B$  of the heading of the barycenter of the group with the wall for fish experiments (red line in all panels), model simulations (panels ABC), and robot experiments (panels DEF), compared to the corresponding null models ( $k = 0$ , no interaction between individuals) in both simulations and robots (gray line in all panels). Curves for agents (fish model and robots) are in blue and gray, depending on the value of  $k$  (see legend in panel B). Interaction strategies involve the  $k$  NEAREST neighbors (panels AD),  $k$  RANDOM neighbors (panels BE), and the  $k$  MOST INFLUENTIAL neighbors (panels CF).

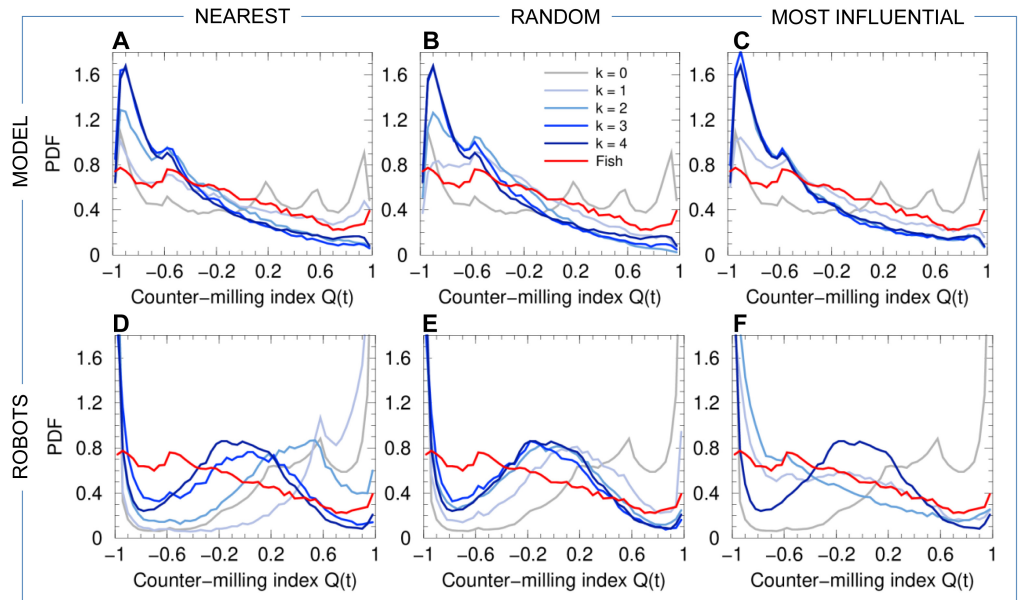


**Fig 8. Counter-milling index.** PDF of the counter-milling index  $Q$  for fish experiments (red line in all panels), model simulations (panels ABC), and robot experiments (panels DEF), compared to the corresponding null models ( $k = 0$ , no interaction between individuals) in both simulations and robots (gray line in all panels). Curves for agents (fish model and robots) are in blue and gray, depending on the value of  $k$  (see legend in panel B). Interaction strategies involve the  $k$  NEAREST neighbors (panels AD),  $k$  RANDOM neighbors (panels BE), and the  $k$  MOST INFLUENTIAL neighbors (panels CF).

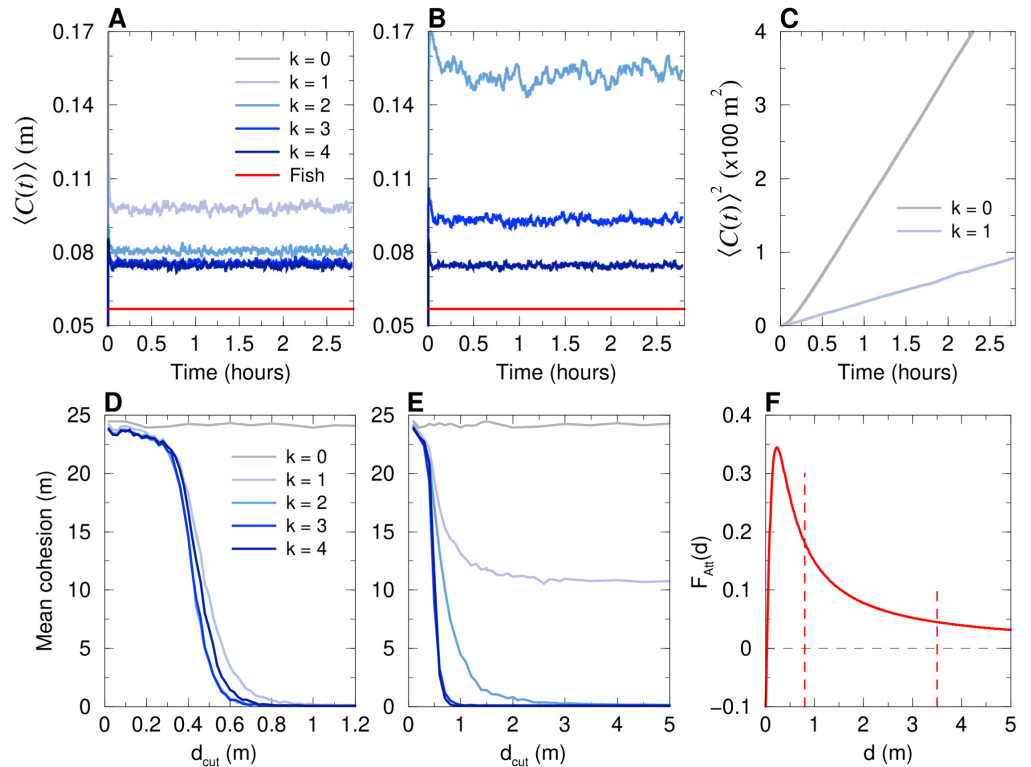


**Fig 9. Average cohesion of a group of 5 agents swimming in an unbounded domain.** Model simulations for the MOST INFLUENTIAL strategy (AD) and the NEAREST strategy (BCE), for  $k = 1, \dots, 4$  (blue lines), together with the case with no interaction ( $k = 0$ , gray lines) and the mean cohesion for fish experiments (red lines in AB). For  $k = 0$ , cohesion is lost immediately, so that the gray line is not visible on the scale of panels AB. (C): Squared mean cohesion in the diffusive cases for  $k = 1$  nearest neighbor and  $k = 0$ . (ABC): Average over 1000 runs with 10000 kicks ( $\approx 2.7$  hours) per run. (DE): Mean cohesion averaged over the last 10% of the 1000 runs for different values of the cut-off distance  $d_{\text{cut}}$  for the two strategies: (D) MOST INFLUENTIAL, and (E) NEAREST. Panel (F): We plot the attraction function  $F_{\text{Att}}$  (see Eq. 10), showing the critical values  $d_{\text{cut}}^*$  above which cohesion is preserved (vertical dashed lines):  $d_{\text{cut}}^* \sim 0.8$  m when the interacting neighbors are the  $k = 1, 2$  or  $3$  most influential ones, the  $k = 3$  nearest ones, or all the neighbors ( $k = 4$ );  $d_{\text{cut}}^* \approx 3.5$  m when interacting with the  $k = 2$  nearest neighbors ( $d_{\text{cut}}^*$  does not exist when interacting only with the nearest neighbor).

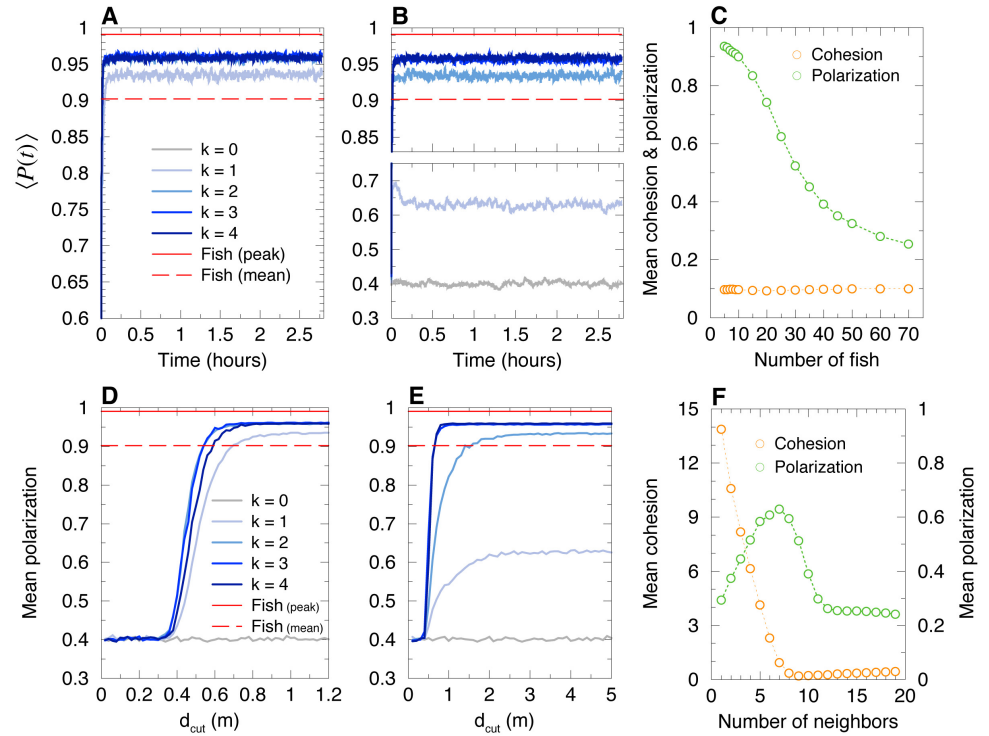


**Fig 10. Average polarization of groups of 5 agents, and mean cohesion and polarization in larger groups ( $N = 5, \dots, 70$ ), when agents are swimming in an unbounded domain.** For  $N = 5$ , model simulations for the MOST INFLUENTIAL strategy (AD) and the NEAREST strategy (BE), for  $k = 1, \dots, 4$  (blue lines), together with the case with no interaction ( $k = 0$ , gray lines) and the mean polarization for fish experiments (red lines). Panel (C): Mean cohesion and polarization in large groups ( $N = 5, \dots, 70$ ) for the MOST INFLUENTIAL strategy ( $k = 1$ ). Panel (F): Mean cohesion and polarization in a group of size  $N = 20$  as a function of the number  $k$  of nearest neighbors with which focal individuals interact. The minimum of the cohesion is reached at  $k = 9$ , and the maximum of the polarization at  $k = 7$ .

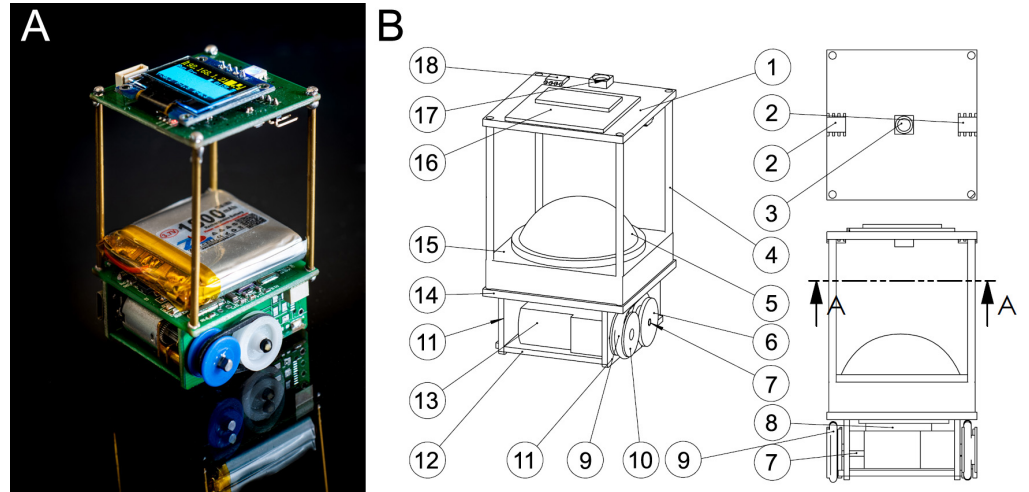


**Fig 11. Cuboid robots.** (A) Photograph of a Cuboid robot. Credits to David Villa ScienceImage/CBI/CNRS, Toulouse, 2018. (B) Design structure of Cuboid robot; A-A represents a cutaway view.

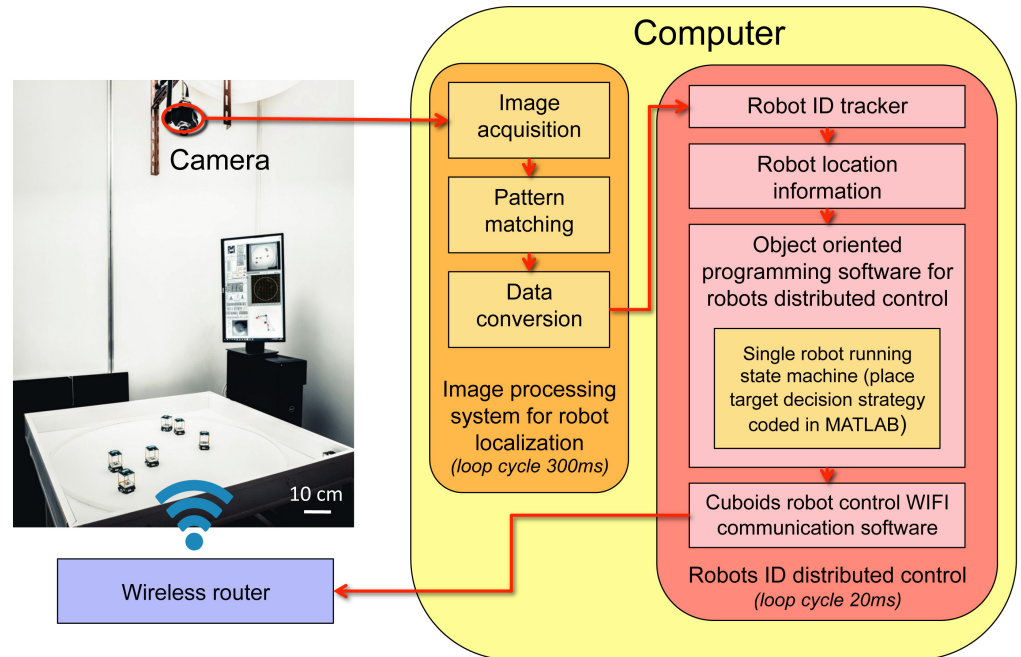


**Fig 12. Structure of Cuboids platform.** Two main parts: the physical hardware and the control software. The hardware consists of a square platform. A camera mounted on the top of it monitors the movements of Cuboids robots, which are controlled in a distributed way by a wireless router. The software processes the image acquired by the camera, then computes the command of actions to be performed by each robot, and finally sends the control signals to the robots via the WIFI channel. Then, all the robots execute their commands at the same time to perform the collective motion. The WIFI broadcasting is one-way communication for sending the command to the robots every 20 ms. In this setup, no information acquired by robots sensors is sent back to the computer though the WIFI channel. Credits to David Villa ScienceImage/CBI/CNRS, Toulouse, 2018.

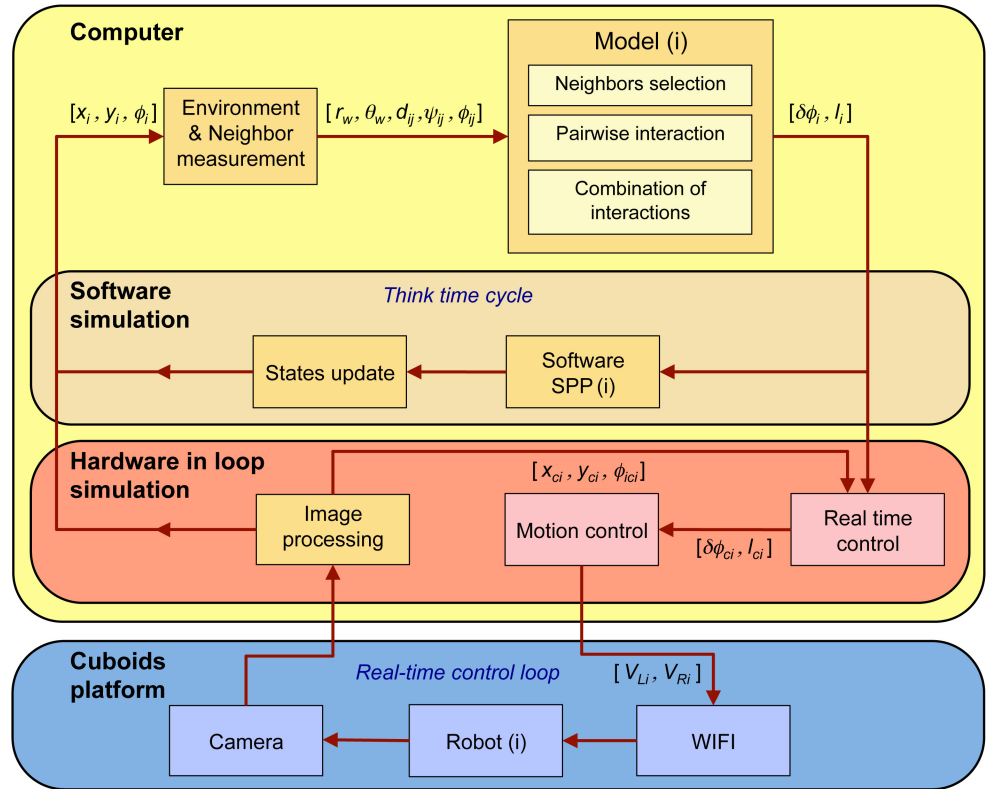


**Fig 13. Software simulation and Hardware in Loop (HIL) simulation (from [42]).** The structure of HIL is an extension of the software simulation, which consists of two extra parts: 1) a computer software (Image Processing, Motion Control, and Real Time Control modules) and 2) a physical hardware (Robot, camera and wireless router). In the software simulation, the Environment & Neighbor Measurement module converts the global position of a robot or a particle  $(x_i, y_i, \phi_i)$  in the SPP software into local information  $(r_{w,i}, \theta_{w,i})$  and  $(d_{ij}, \psi_{ij}, \phi_{ij})$ . Then the computational model generates a new kick decision in the form of heading variation and kick length  $(\delta\phi_i, l_i)$ . This new decision  $(\delta\phi_i, l_i)$  is then directly sent to the SPP(i) software. Once the state has been updated, a new global position is provided by the SPP(i) software (brown box) or the Hardware in loop simulation (red box). By contrast, the HIL simulation includes hardware, *i.e.*, robots, camera and WIFI router (blue box). Furthermore, each robot  $i$  is controlled in real time by three more software modules running in the computer, which are the *Image Processing*, *Motion Control*, and *Real Time Control* modules (red box). The Image Processing module computes the global position of each robot  $(x_{c,i}, y_{c,i}, \phi_{c,i})$  from the information provided by the camera in real time. Then, the Real Time Control module converts the model decision  $(\delta\phi_i, l_i)$  into a real time decision in the robot  $(\delta\phi_{c,i}, l_{c,i})$ , which are the heading variation and kick length to perform the decision based on its real time position  $(x_{c,i}, y_{c,i}, \phi_{c,i})$ . Finally, the Motion Control software generates left and right wheel motors speed control  $(V_{L,i}, V_{R,i})$  for each robot to achieve its decision  $(\delta\phi_{c,i}, l_{c,i})$ . Each robot receives these motor commands by WIFI signals, and performs the corresponding movements that are monitored by the camera.

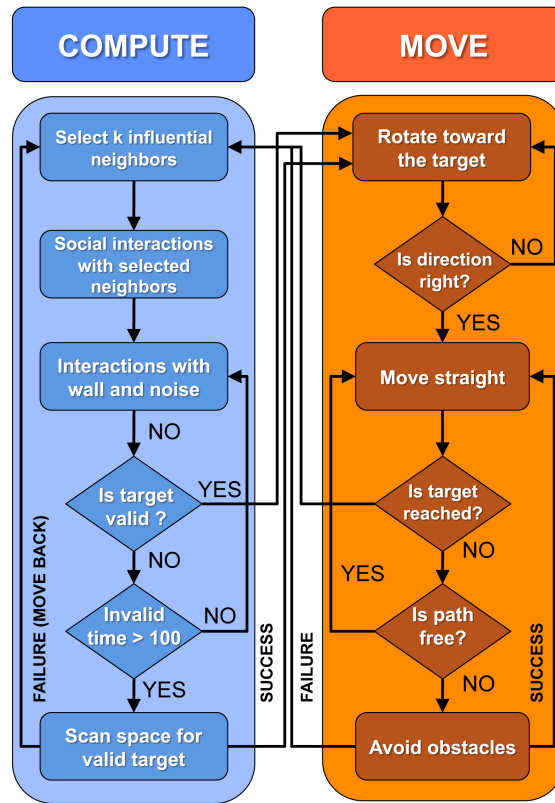


**Fig 14. Flow chart of robot states machine.** At any time a robot can be in one of the two following states: (1) the COMPUTE state for choosing a new target place, and (2) the MOVE state to reach the target place. In the COMPUTE state, the robot first selects influential neighbors, then it computes the pairwise influence of each neighbor, and finally it adds all influences to generate a new target place. Then, this new target place is validated to avoid collisions with the wall or another robot. If a valid target place cannot be found, the robot scans all space around itself for a valid target place. If the scanning method cannot find a valid target, the robot moves back over a distance of 80 mm and starts again the COMPUTE state. When a valid target place has been found, the robot switches into the MOVE state. The robot first rotates toward the target and then, moves straight to it. If another running neighbor blocks the path, the robot uses a procedure to avoid the obstacles.

STRATEGY		$C$	$P$	$r_w^B$	$\theta_w^B$	$Q$	$\langle \text{All} \rangle$
	$k = 0$	0.909	0.532	0.341	0.145	0.023	0.390
NEAREST	$k = 1$	0.369	0.178	0.034	0.041	0.003	0.125
	$k = 2$	0.065	0.049	0.032	0.033	0.020	0.040
	$k = 3$	0.013	0.026	0.027	0.032	0.037	0.027
RANDOM	$k = 1$	0.310	0.223	0.095	0.068	0.009	0.141
	$k = 2$	0.061	0.103	0.037	0.059	0.037	0.059
	$k = 3$	0.012	0.062	0.028	0.048	0.038	0.038
MOST INFLU- ENTIAL	$k = 1$	0.078	0.150	0.067	0.048	0.006	0.070
	$k = 2$	0.011	0.051	0.025	0.080	0.033	0.040
	$k = 3$	0.016	0.038	0.027	0.042	0.036	0.032
	$k = 4$	0.014	0.042	0.024	0.044	0.030	0.031

**Table 1. Model simulations vs fish experiments.** Distance  $D(\text{Fish} | \text{Model})$  between the probability distribution function (PDF) of the 5 observables used to quantify the collective motion in the fish model and the corresponding PDF obtained in fish experiments. We list the results for the 3 different interaction strategies implemented in the fish model and the associated value of  $k$  for the number of interacting neighbors. The last column  $\langle \text{All} \rangle$  corresponds to the average of the 5 corresponding distances, an arbitrary but reasonable global quantifier to assess the overall agreement of a given condition with the results of fish experiments. For  $k = 1$ , the MOST INFLUENTIAL strategy gives significantly better results than the two other strategies and already leads to a fair agreement with fish experiments.

STRATEGY		$C$	$P$	$r_w^B$	$\theta_w^B$	$Q$	$\langle \text{All} \rangle$
	$k = 0$	0.604	0.561	0.238	0.114	0.170	0.337
NEAREST	$k = 1$	0.418	0.486	0.158	0.070	0.239	0.274
	$k = 2$	0.111	0.249	0.063	0.042	0.093	0.112
	$k = 3$	0.066	0.039	0.083	0.036	0.026	0.05
RANDOM	$k = 1$	0.140	0.343	0.040	0.107	0.065	0.139
	$k = 2$	0.019	0.141	0.035	0.080	0.029	0.061
	$k = 3$	0.056	0.063	0.095	0.042	0.025	0.056
MOST INFLUENTIAL	$k = 1$	0.045	0.089	0.050	0.042	0.011	0.047
	$k = 2$	0.028	0.050	0.031	0.088	0.024	0.044
	$k = 4$	0.078	0.080	0.040	0.053	0.038	0.058

**Table 2. Collective robotics experiments vs fish experiments.** Distance  $D(\text{Fish} | \text{Robots})$  between the probability distribution function (PDF) of the 5 observables used to quantify the collective motion of the robots and the corresponding PDF obtained in fish experiments. We list the results for the 3 different interaction strategies implemented in the fish model and the associated value of  $k$  for the number of interacting neighbors. The last column  $\langle \text{All} \rangle$  corresponds to the average of the 5 corresponding distances, an arbitrary but reasonable global quantifier to assess the overall agreement of a given condition with the results of fish experiments. For  $k = 1$ , the MOST INFLUENTIAL strategy gives significantly better results than the two other strategies and already leads to a fair agreement with fish experiments.

Parameter	Symbol	Model	Robots
Intensity of heading random fluctuations	$\gamma_R$	0.45	0.1
Fluctuations reduction factor when close to wall	$\alpha$	0.67	1
Intensity of wall repulsion	$\gamma_w$	0.15	0.79
Range of wall repulsion (cm)	$l_w$	6	11
Intensity of attraction/repulsion	$\gamma_{Att}$	0.12	0.18
Range of attraction between individuals (cm)	$l_{Att}$	20	37
Distance of balance of attraction/repulsion (cm)	$d_{Att}$	3	18
Intensity of alignment	$\gamma_{Ali}$	0.09	0.04
Range of alignment between individuals (cm)	$l_{Ali}$	20	37
Distance of alignment (cm)	$d_{Ali}$	6	5
Average duration between successive kicks (s)	$\tau$	0.5	1.3
Mean length between two successive kicks (cm)	$l$	7	7.4
Typical individual velocity in active period (cm/s)	$v_0$	14	3.75
Relaxation time (s)	$\tau_0$	0.8	0.9

**Table 3.** Values and units of the parameters for model simulations and robot experiments.

1372 **Supporting Information**

1373 **Supporting figures**

1374 **S1 Fig. Density maps of the polarization vs cohesion for fish and model**  
 1375 **simulations, normalized with the total number of data.**

1376 Density maps are shown for fish experiments (FISH panel) and for the 11 strategies  
 1377 considered in the model simulations. The color intensity corresponds to the number of  
 1378 data in each box normalized with the total number of data in the grid ( $\times 1000$ ). We  
 1379 used  $40 \times 50$  boxes.

1380 **S2 Fig. Density maps of polarization vs cohesion for fish and model simu-**  
 1381 **lations, normalized with the number of data per range of polarization.**

1382 Density maps are shown for fish experiments (FISH panel) and for the 11 strategies  
 1383 considered in the model simulations. The color intensity corresponds to the number of  
 1384 data in each box normalized with the number of data per interval of polarization, *i.e.*,  
 1385 each row is the PDF of the cohesion for a range of values of the polarization. We used  
 1386  $40 \times 50$  boxes.

1387 **S3 Fig. Density maps of polarization vs cohesion for fish and robot groups,**  
 1388 **normalized with the total number of data.**

1389 Density maps are shown for fish experiments (FISH panel) and for the 10 strategies  
 1390 considered in the robot experiments. The color intensity corresponds to the number of  
 1391 data in each box normalized with the total number of data in the grid ( $\times 1000$ ). We  
 1392 used  $40 \times 50$  boxes.

1393 **S4 Fig. Density maps of polarization vs cohesion for fish and robot groups,**  
 1394 **normalized with the number of data per range of polarization.**

1395 Density maps are shown for fish experiments (FISH panel) and for the 10 strategies  
 1396 considered in the robot experiments. The color intensity corresponds to the number of  
 1397 data in each box normalized with the number of data per interval of polarization, *i.e.*,  
 1398 each row is the PDF of the cohesion for a range of values of the polarization. We used  
 1399  $40 \times 50$  boxes.

1400 **S5 Fig. Counter-milling in model simulations.** Red arrows represent the velocity  
 1401 field of agents in the reference system of the barycenter of the group, here located at  
 1402 coordinates  $(0, 0)$ . Orange circle denotes the average relative position of the border of  
 1403 the arena with respect to the barycenter. The cases where agents interact with the  $k = 3$   
 1404 most influential neighbors (statistically identical to the case where  $k = 4$ ) and where  
 1405 agents do not interact ( $k = 0$ ) are not shown.

1406 **S6 Fig. Counter-milling in robotic experiments.** Red arrows represent the  
 1407 velocity field of robots in the reference system of the barycenter of the group, here  
 1408 located at coordinates  $(0, 0)$ . Orange circle denotes the average relative position of the  
 1409 border of the arena with respect to the barycenter. The cases where robots interact with  
 1410 the  $k = 3$  most influential neighbors (statistically identical to the case where  $k = 4$ ) and  
 1411 where robots do not interact ( $k = 0$ ) are not shown.

1412 **S7 Fig. Average cohesion and polarization for group sizes  $N = 5, \dots, 20$**   
 1413 **( $N$  even) when each individual interacts with its  $k$  nearest neighbors, for**  
 1414  **$k = 1, \dots, N - 1$ .** Mean cohesion (A) and mean polarization (B) as a function of  $k$ .  
 1415 Cohesion values are scaled with  $\lambda_M = 0.87$ . In panel (A), high values of the cohesion for  
 1416 small values of  $k$  with respect to the group size  $N$  are not shown (vertical lines grow up  
 1417 to 20 m in our simulations as the individuals diffuse independently of each other). In  
 1418 (B), the values of  $k$  for  $N = 22, 24$  and  $26$  (marked with an asterisk in the legend) are  
 1419 limited to the interval of interest [8, 12].

1420 **S8 Fig. Finite state machine diagram of one robot.** The decision-making  
 1421 processes of the robot (COMPUTE state) are shown in blue. The movements of the  
 1422 robot (MOVE state) are shown in brown. In the COMPUTE state, the model determines  
 1423 a new target to reach by integrating the local information about the neighbors and the  
 1424 environment. A target is valid when this one is not blocked by the wall or other robots.  
 1425 If the target is invalid, the computer tries to find a new target by the scanning method.  
 1426 If the scanning fails, the robot moves back 80 mm and starts again for model computing.  
 1427 If the decision target is valid, the robot switches into MOVE state, which includes three  
 1428 sub-states: Rotate, Move straight, and Avoid obstacle. The robot first rotates towards  
 1429 to the target and then moves straight to it. If a running neighbor blocks the path, the  
 1430 robot uses a procedure to avoid the obstacle.

1431 **S9 Fig. Interaction functions with the wall and between individuals, ex-**  
 1432 **tracted from experiments of fish swimming in pairs [14].** (A) Intensity of the  
 1433 repulsion from the wall  $F_w(r_{w,i})$  (green) as a function of the distance to the wall  $r_{w,i}$ ,  
 1434 and intensity of the attraction  $F_{Att}(d_{ij})$  (red) and the alignment  $F_{Ali}(d_{ij})$  (blue) between  
 1435 fish  $i$  and  $j$  as functions of the distance  $d_{ij}$  separating them. (B) Normalized odd angular  
 1436 function  $O_w(\theta_{w,i})$  modulating the interaction with the wall as a function of the relative  
 1437 angle to the wall  $\theta_{w,i}$ . (C) Normalized angular functions  $O_{Att}(\psi_{ij})$  (odd, in red) and  
 1438  $E_{Att}(\phi_{ij})$  (even, in orange) of the attraction interaction, and (D)  $O_{Ali}(\phi_{ij})$  (odd, in blue)  
 1439 and  $E_{Ali}(\psi_{ij})$  (even, in violet) of the alignment interaction between agents  $i$  and  $j$ , as  
 1440 functions of the angle of perception  $\psi_{ij}$  and the relative heading  $\phi_{ij}$ .

## 1441 Supporting videos

1442 **S1 Video. Collective movements in rummy-nose tetra (*Hemigrammus rhodos-***  
 1443 ***tomus*).** A typical experiment with a group of 5 fish swimming in a circular tank of  
 1444 radius 250 mm.

1445 **S2 Video. Collective motion in a group of 5 robots.** Each robot interacts with  
 1446 its most influential neighbor. The video is accelerated 9 times. Total duration: 7.15  
 1447 minutes.

1448 **S3 Video. Tracking and analysis output.** The small circles superimposed on  
 1449 the trajectories represents the kicks performed by the fish when the speed reaches its  
 1450 maximum value.

1451 **S4 Video. Counter milling behavior in a group of 5 fish.** Top: Typical experi-  
 1452 ment with a group of 5 fish in a circular arena of radius 250 mm. The video is accelerated  
 1453 6 times. Total duration 1.3 minutes. Bottom: Relative movement of fish with respect to  
 1454 the barycenter of the group, represented by the black arrow on top video and a black  
 1455 disk on the bottom video. Fish turn counter-clockwise around the tank and clockwise  
 1456 with respect to the barycenter.

1457 **S5 Video. Collective robotics experiment without any social interaction**  
 1458 **between the robots ( $k = 0$ ) and only obstacle avoidance behavior is at play.**  
 1459 Top: Typical experiment with a group of 5 robots in a circular arena of radius 420 mm,  
 1460 captured by the top camera. The border of the arena is represented by the red circle.  
 1461 Purple circles represent the individual robot safety area, of diameter 8 cm. Small green  
 1462 dots in front of robots indicate their next target place. The video is accelerated 6 times.  
 1463 Total duration: 6 minutes. Bottom: Relative movement of the robots with respect to the  
 1464 barycenter of the group. The barycenter is represented by the black disk and remains  
 1465 oriented to the right. Robots are represented by colored disks with their identification  
 1466 number in the center. The small circle at the front of a robot indicates its heading. The  
 1467 arrows represent the interactions between robots. Arrow direction indicates the identity  
 1468 (color) of the robot that exerts its influence on the robot to which the arrow points. The  
 1469 small dots in front of the robots represent the next target places.

1470 **S6 Video. Collective robotics experiment where robots interact with the**  
 1471  **$k = 1$  nearest neighbor.** Top: Typical experiment with a group of 5 robots in a  
 1472 circular arena of radius 420 mm, captured by the top camera. The border of the arena is  
 1473 represented by the red circle. Purple circles represent the individual robot safety area, of  
 1474 diameter 8 cm. Small green dots in front of robots indicate their next target place. The  
 1475 video is accelerated 6 times. Total duration: 6 minutes. Bottom: Relative movement of  
 1476 the robots with respect to the barycenter of the group. The barycenter is represented  
 1477 by the black disk and remains oriented to the right. Robots are represented by colored  
 1478 disks with their identification number in the center. The small circle at the front of  
 1479 a robot indicates its heading. The arrows represent the interactions between robots.  
 1480 Arrow direction indicates the identity (color) of the robot that exerts its influence on  
 1481 the robot to which the arrow points. The small dots in front of the robots represent the  
 1482 next target places.

1483 **S7 Video. Collective robotics experiment where robots interact with the**  
 1484  **$k = 1$  most influential neighbor.** Top: Typical experiment with a group of 5 robots  
 1485 in a circular arena of radius 420 mm, captured by the top camera. The border of the  
 1486 arena is represented by the red circle. Purple circles represent the individual robot safety  
 1487 area, of diameter 8 cm. Small green dots in front of robots indicate their next target  
 1488 place. The video is accelerated 6 times. Total duration: 6 minutes. Bottom: Relative  
 1489 movement of the robots with respect to the barycenter of the group. The barycenter is  
 1490 represented by the black disk and remains oriented to the right. Robots are represented  
 1491 by colored disks with their identification number in the center. The small circle at the  
 1492 front of a robot indicates its heading. The arrows represent the interactions between  
 1493 robots. Arrow direction indicates the identity (color) of the robot that exerts its influence  
 1494 on the robot to which the arrow points. The small dots in front of the robots represent  
 1495 the next target places.

1496 **S8 Video. Collective robotics experiment where robots interact with  $k = 1$**   
 1497 **randomly selected neighbor.** Top: Typical experiment with a group of 5 robots in a  
 1498 circular arena of radius 420 mm, captured by the top camera. The border of the arena is  
 1499 represented by the red circle. Purple circles represent the individual robot safety area, of  
 1500 diameter 8 cm. Small green dots in front of robots indicate their next target place. The  
 1501 video is accelerated 6 times. Total duration: 6 minutes. Bottom: Relative movement of  
 1502 the robots with respect to the barycenter of the group. The barycenter is represented  
 1503 by the black disk and remains oriented to the right. Robots are represented by colored  
 1504 disks with their identification number in the center. The small circle at the front of  
 1505 a robot indicates its heading. The arrows represent the interactions between robots.  
 1506 Arrow direction indicates the identity (color) of the robot that exerts its influence on  
 1507 the robot to which the arrow points. The small dots in front of the robots represent the  
 1508 next target places.

1509 **S9 Video. Collective robotics experiment where robots interact with the**  
 1510  **$k = 2$  nearest neighbors.** Top: Typical experiment with a group of 5 robots in a  
 1511 circular arena of radius 420 mm, captured by the top camera. The border of the arena is  
 1512 represented by the red circle. Purple circles represent the individual robot safety area, of  
 1513 diameter 8 cm. Small green dots in front of robots indicate their next target place. The  
 1514 video is accelerated 6 times. Total duration: 6 minutes. Bottom: Relative movement of  
 1515 the robots with respect to the barycenter of the group. The barycenter is represented  
 1516 by the black disk and remains oriented to the right. Robots are represented by colored  
 1517 disks with their identification number in the center. The small circle at the front of  
 1518 a robot indicates its heading. The arrows represent the interactions between robots.  
 1519 Arrow direction indicates the identity (color) of the robot that exerts its influence on  
 1520 the robot to which the arrow points. The small dots in front of the robots represent the  
 1521 next target places.

1522 **S10 Video. Collective robotics experiment where robots interact with the**  
 1523  **$k = 2$  most influential neighbors.** Top: Typical experiment with a group of 5 robots  
 1524 in a circular arena of radius 420 mm, captured by the top camera. The border of the  
 1525 arena is represented by the red circle. Purple circles represent the individual robot safety  
 1526 area, of diameter 8 cm. Small green dots in front of robots indicate their next target  
 1527 place. The video is accelerated 6 times. Total duration: 6 minutes. Bottom: Relative  
 1528 movement of the robots with respect to the barycenter of the group. The barycenter is  
 1529 represented by the black disk and remains oriented to the right. Robots are represented  
 1530 by colored disks with their identification number in the center. The small circle at the  
 1531 front of a robot indicates its heading. The arrows represent the interactions between  
 1532 robots. Arrow direction indicates the identity (color) of the robot that exerts its influence  
 1533 on the robot to which the arrow points. The small dots in front of the robots represent  
 1534 the next target places.

1535 **S11 Video. Collective robotics experiment where robots interact with  $k = 2$**   
 1536 **randomly selected neighbors.** Top: Typical experiment with a group of 5 robots in  
 1537 a circular arena of radius 420 mm, captured by the top camera. The border of the arena  
 1538 is represented by the red circle. Purple circles represent the individual robot safety area,  
 1539 of diameter 8 cm. Small green dots in front of robots indicate their next target place.  
 1540 The video is accelerated 6 times. Total duration: 6 minutes. Bottom: Relative movement  
 1541 of the robots with respect to the barycenter of the group. The barycenter is represented

1542 by the black disk and remains oriented to the right. Robots are represented by colored  
 1543 disks with their identification number in the center. The small circle at the front of  
 1544 a robot indicates its heading. The arrows represent the interactions between robots.  
 1545 Arrow direction indicates the identity (color) of the robot that exerts its influence on  
 1546 the robot to which the arrow points. The small dots in front of the robots represent the  
 1547 next target places.

1548 **S12 Video. Collective robotics experiment where robots interact with the**  
 1549  **$k = 3$  nearest neighbors.** Top: Typical experiment with a group of 5 robots in a  
 1550 circular arena of radius 420 mm, captured by the top camera. The border of the arena is  
 1551 represented by the red circle. Purple circles represent the individual robot safety area, of  
 1552 diameter 8 cm. Small green dots in front of robots indicate their next target place. The  
 1553 video is accelerated 6 times. Total duration: 6 minutes. Bottom: Relative movement of  
 1554 the robots with respect to the barycenter of the group. The barycenter is represented  
 1555 by the black disk and remains oriented to the right. Robots are represented by colored  
 1556 disks with their identification number in the center. The small circle at the front of  
 1557 a robot indicates its heading. The arrows represent the interactions between robots.  
 1558 Arrow direction indicates the identity (color) of the robot that exerts its influence on  
 1559 the robot to which the arrow points. The small dots in front of the robots represent the  
 1560 next target places.

1561 **S13 Video. Collective robotics experiment where robots interact with  $k = 3$**   
 1562 **randomly selected neighbors.** Top: Typical experiment with a group of 5 robots in  
 1563 a circular arena of radius 420 mm, captured by the top camera. The border of the arena  
 1564 is represented by the red circle. Purple circles represent the individual robot safety area,  
 1565 of diameter 8 cm. Small green dots in front of robots indicate their next target place.  
 1566 The video is accelerated 6 times. Total duration: 6 minutes. Bottom: Relative movement  
 1567 of the robots with respect to the barycenter of the group. The barycenter is represented  
 1568 by the black disk and remains oriented to the right. Robots are represented by colored  
 1569 disks with their identification number in the center. The small circle at the front of  
 1570 a robot indicates its heading. The arrows represent the interactions between robots.  
 1571 Arrow direction indicates the identity (color) of the robot that exerts its influence on  
 1572 the robot to which the arrow points. The small dots in front of the robots represent the  
 1573 next target places.

1574 **S14 Video. Collective robotics experiment where robots interact with all**  
 1575 **their neighbors ( $k = 4$ ).** Top: Typical experiment with a group of 5 robots in a  
 1576 circular arena of radius 420 mm, captured by the top camera. The border of the arena is  
 1577 represented by the red circle. Purple circles represent the individual robot safety area, of  
 1578 diameter 8 cm. Small green dots in front of robots indicate their next target place. The  
 1579 video is accelerated 6 times. Total duration: 6 minutes. Bottom: Relative movement of  
 1580 the robots with respect to the barycenter of the group. The barycenter is represented  
 1581 by the black disk and remains oriented to the right. Robots are represented by colored  
 1582 disks with their identification number in the center. The small circle at the front of  
 1583 a robot indicates its heading. The arrows represent the interactions between robots.  
 1584 Arrow direction indicates the identity (color) of the robot that exerts its influence on  
 1585 the robot to which the arrow points. The small dots in front of the robots represent the  
 1586 next target places.